Clays and Clay Minerals, Vol. 58, No. 5, 606–626, 2010.

SAPONITE-RICH BLACK SHALES AND NONTRONITE BEDS OF THE PERMIAN IRATI FORMATION: SEDIMENT SOURCES AND THERMAL METAMORPHISM (PARANÁ BASIN, BRAZIL)

Camila Wense Dias Dos Anjos[1,2], Alain Meunier[1], Edi Mendes Guimarães[2], and Abderrazzak el Albani[1,*]

[1] Université de Poitiers-UMR6269-INSU CNRS, HydrASA, 40 Avenue Recteur Pineau, Poitiers, 86022, France
[2] Universidade de Brasília, Instituto de Geociências, Brasília, 70910-900, Brazil

Abstract—Shales and claystones in the Permian Irati Formation consist of Al-rich or Fe-Mg clay minerals in its southern/central and northern parts, respectively. The constrasting compositions indicate particular geological and paleo-environmental conditions. The purpose of this study was to determine the conditions of formation by characterizing the black shales and claystones from different sections of the northern edge of the basin, some of which reveal the presence of intruded diabase sills.

Black shales consist of saponite or saponite-talc mixed layers, talc, lizardite, nontronite, and quartz. Green claystones are nontronite-rich but also contain lizardite, talc, and quartz. The chemical compositions of the black shale and claystones, except for one sample (POR-56), exhibit a positive correlation of the TiO_2, Cr, and P_2O_5 contents with Al_2O_3, which typically results from weathering processes. The presence of saponite, nontronite, and some accessory minerals (spinel, pyroxene, native silver) suggests altered basic-ultrabasic rocks as sediment sources, consistent with the rare earth element (*REE*) composition being less than the Post-Archean Average Shale (PAAS) or North American Shale Composite (NASC) levels and with negative Ce and Eu anomalies. Sample POR-56 consists largely of nontronite and is anomalously rich in zircon, monazite, and apatite. Chemically, sample POR-56 is different from the black shales and claystones, being richer in Al_2O_3-Fe_2O_3, MgO-poor, and having greater *REE* contents than the PAAS or NASC standards. The POR-56 bed is probably a bentonite resulting from the alteration of volcanic ash in sea water (strong, negative Ce anomaly). The Zr/TiO_2 *vs*. Nb/Y relation indicates that the magmatism was andesitic. During the Upper Permian, intermediate to basic volcanic activity was recorded in the Mitu Group of the Central Andes.

Close to the diabase sill, the black shales and claystones contain saponite, talc, and lizardite but nontronite is absent. Saponite and talc crystals, however, exhibit a larger coherent scattering domain size (CSDS) and are randomly oriented with respect to the sedimentary bedding. The thermal metamorphism effect is confirmed by the presence of secondary enstatite-augite and albite crystals.

Key Words—Ash Fall Level, Black Shales, Bazil, Genesis, Nontronite, Paraná Basin, Saponite, Sediment Source, Talc, Thermal Metamorphism.

INTRODUCTION

Black shales from the Irati Formation in the Paraná basin (south-central Brazil and Uruguay) consist mainly of aluminous-rich clay minerals such as illite or illite-smectite mixed-layer minerals (I-S) in the central and southern parts (Ramos and Formoso, 1976; Rodrigues and Quadros, 1976; Santos Neto, 1993; Maynard *et al.*, 1996) and of Mg- and Fe-rich clay minerals in the northern part of the formation (Dos Anjos, 2003). This composition may be due either to different sediment sources or to specific paleo-environments favoring the formation of Fe-Mg clays. Indeed, Mg- and Fe-rich clay minerals formed in surface conditions may originate from: (1) weathering of mafic-ultramafic rocks (Eggleton and Boland, 1982; Nahon *et al.*, 1982; Fontanaud and Meunier, 1983; Noack and Duplay, 1983; Colin *et al.*, 1990; Noack *et al.*, 1993; Keeling *et al.*, 2000; Velde and Meunier, 2008); (2) precipitation in confined sea water (Rehim *et al.*, 1986; Chamley, 1989; Karakaya *et al.*, 2004; Sakharov *et al.*, 2004; Yalçin and Bozkaya, 2006), or (3) precipitation in lacustrine environments (Akbulut and Kadir, 2003; Bristow *et al.*, 2009). Each of the three possible origins implies mineralogical and chemical characteristics of the sediments. The aim of the present work was to determine the genetic signatures.

To determine the origin of the Fe- and Mg-rich clay minerals, the present work presents a petrographical, mineralogical, and geochemical study of black shales and claystones in the northern part of the Paraná Basin. These sediments are interbedded within marls and limestones in the studied sections, some of them containing diabase sills of a few meters to 200 m thick. The volcanic bodies intruded all the sedimentary formations during the early Creatceous (Petri and Fúlfaro, 1983). Consequently, potential metamorphic effects must be taken into account

* E-mail address of corresponding author:
abder.albani@univ-poitiers.fr
DOI: 10.1346/CCMN.2010.0580503

before determining the mineralogical or chemical signature of the sediments.

GEOLOGICAL SETTINGS

The geological framework of the Paraná Basin

The Permian Irati Formation is a black shale-carbonate sequence of the Paraná Basin, a large intracratonic basin located in the central–eastern part of the South America Platform (Figure 1). This basin was filled from the Late Ordovician to the Late Cretaceous by six, second-order, sedimentary-magmatic supersequences (Milani, 1997): Rio Ivaí (Ordovician–Silurian); Paraná (Devonian); Gondwana I (Carboniferous–Permian); Gondwana II (Triassic); Gondwana III (Jurassic–Cretaceous); and Bauru (Cretaceous). The Rio Ivaí, Paraná, and Gondwana I supersequences represent Paleozoic transgressive-regressive cycles. The Gondwana II, Gondwana III, and Bauru supersequences are composed of continental sedimentary series associated with igneous rocks.

Based on sedimentological, stratigraphical, geochemical, and palynological data, the Irati Formation (Gondwana I supersequence) is considered to have been deposited in a mixed siliciclastic and carbonate marine ramp system. A sea-restricted environment

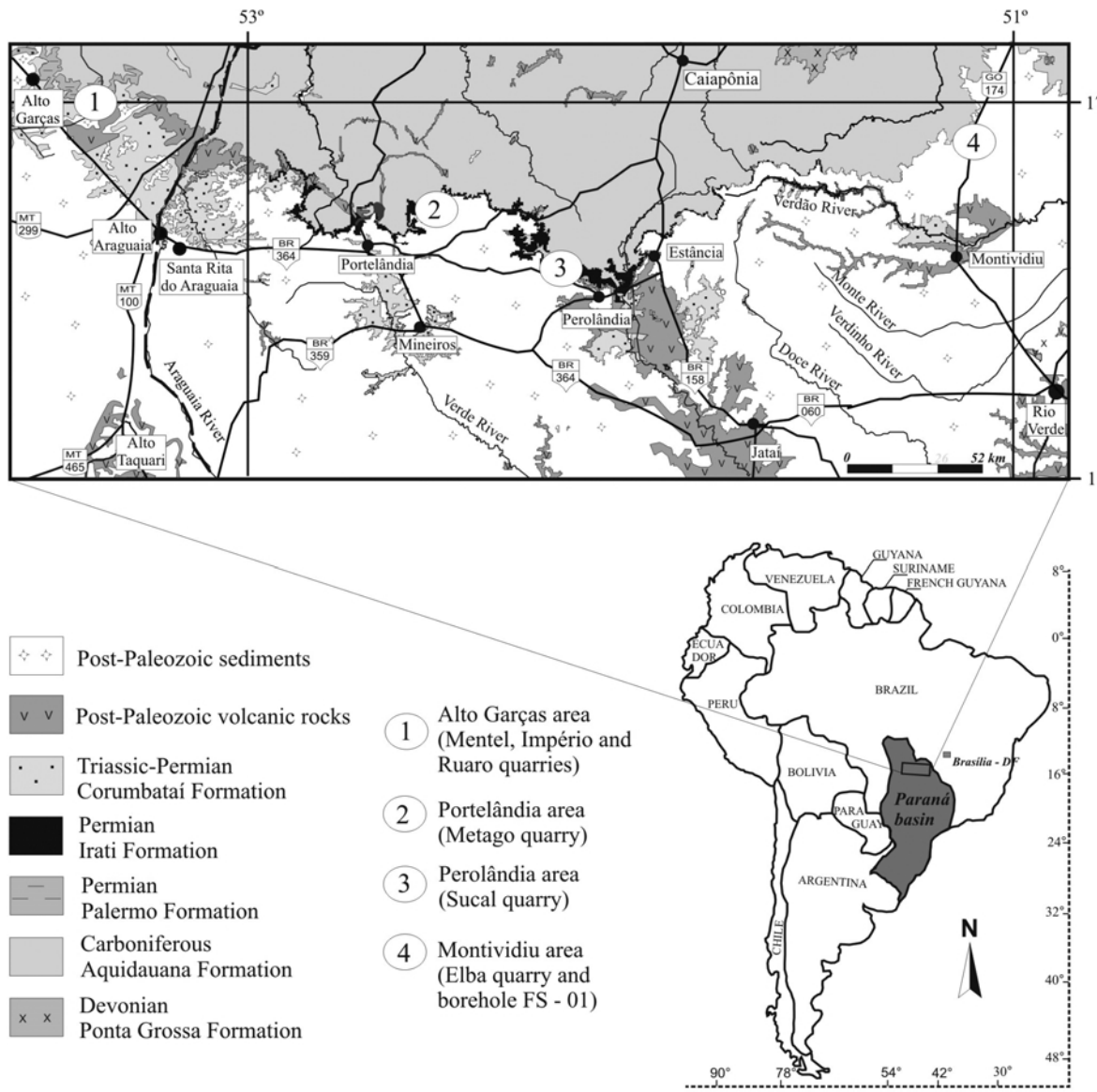

Figure 1. Geological map showing the Irati Formation in the north of the Paraná basin. The location of the quarries and borehole studied are given by numbers.

https://doi.org/10.1346/CCMN.2010.0580503 Published online by Cambridge University Press

prevailed but a link with the Panthalassa ocean was opened in the southern portion of the basin (Sanford and Lange 1960; Santos Neto, 1993; Milani and Thomaz Filho, 2000). In the northeastern part of the basin (State of São Paulo, Brazil), ~900 km from the study area, mm- to cm-thick layers of gypsum and nodular anhydrite indicate confined evaporitic conditions (Santos Neto, 1993). The unit contains typical Gondwana fossils such as the *Glossopteris* flora (White, 1908) and the mesosaur fauna (Mac Gregor, 1908). Fish remains, ostracods, and gastropod shells are also important fossil records sometimes forming coquinas.

The Irati Formation is 40 m thick on average (Mendes *et al.*, 1966). It is subdivided into Taquaral and Assistência members (Barbosa and Gomes, 1958). The Taquaral Member is formed of gray claystones deposited on a basal conglomerate which marks the beginning of the deposition of the sedimentary series. Near the top, the Assistência Member consists of dolostones and limestones alternating with dark-gray to black shales which contain up to 30% organic matter (Pádula, 1968). Organic geochemistry data for the Irati Formation black shales reveal that these rocks were not buried deeply; the maximum burial depth was 2−3 km (Araújo *et al.*, 1996). Considering a gradient of 20ºC/km and a mean surface temperature of 20ºC, Araújo *et al.* (1996) estimated a maximum burial temperature of 60 to 80ºC.

All the Pre-Cretaceous units of the Paraná basin contain igneous intrusions related to the Serra Geral magmatism event which occurred over the period 138−127 Ma (Gomes, 1959). The heat diffusing from the sills into the organic-rich rocks of the Irati Formation triggered synchronous processes of hydrocarbon generation and migration characterizing an atypical petroleum system (Araújo *et al.*, 1996). The heat also activated reactions which changed significantly the mineral assemblages of the sedimentary rocks. In the northeastern part of the Paraná basin, the temperature increase was sufficiently high for pyroxene and chlorite to form in the sedimentary rocks (Amaral, 1970; Girardi *et al.*, 1978). Pyroxene, serpentine, and talc have been observed in claystones and carbonate rocks in the northern part of the basin (Sucal quarry) in the vicinity of a 13 m diabase sill (Dos Anjos, 2003). These host rocks preserved the sedimentary Nd isotopic signature. Their *REE* patterns differ from that of the sill, indicating that the chemical interaction between the igneous and sedimentary rocks was limited. Thus, the effects of the temperature increase during the heat diffusion period

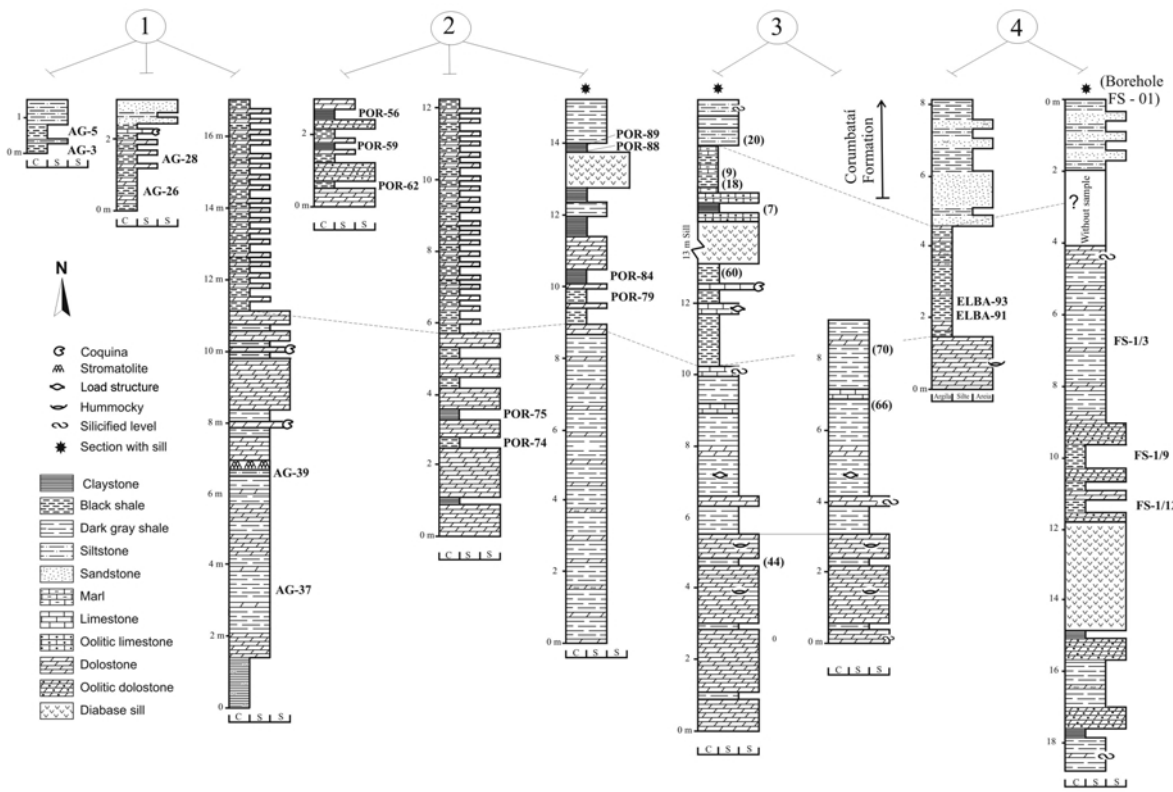

Figure 2. Stratigraphical sections of the Irati Formation in the study area. The numbers correspond to the quarries and borehole locations on the geological map in Figure 1.

https://doi.org/10.1346/CCMN.2010.0580503 Published online by Cambridge University Press

were limited to local mineral metamorphic reactions with no chemical transfers (Santos *et al.*, 2003).

Northern part of the Paraná basin

The Taquaral and Assistência Members are ~10 m and 30 m thick, respectively, in the part of the basin studied (Costa *et al.*, 1981; Rodrigues, 2001). The Taquaral Member consists of a basal, fine conglomerate overlain by white to white-gray, fine sandstones, siltstones, and claystones with intercalations of chert (Rodrigues, 2001). The lower contact of the Taquaral Member with the Aquidauana Formation is marked by an erosional unconformity. The Assistência Member consists largely of an alternation of cm-sized beds of dark gray to black shales and dolostones. Some gray to black claystones, marls, oolitic beds, and a few layers of green to greenish-gray claystones and siltstones occur also. Stromatolitic levels have been observed close to the town of Alto Garças.

At present, the northern part of the basin is surrounded by Archean and Proterozoic rocks of the Paraguay and Brasília fold belts. These units belong to the Tocantins Province, a large Brasiliano/Pan-African orogen formed between the Amazonian, São Francisco/Congo, and Paraná cratons at the end of the Brasiliano Cycle, ~600 Ma ago (Almeida *et al.*, 1981; Pimentel *et al.*, 2000). Metasediments of the Cuiabá Group (Paraguay fold belt) and orthogneisses, meta-volcano-sedimentary series, and post-orogenic granites of the Goiás Magmatic Arc (Brasília fold belt) crop out at the northern border of the Paraná basin.

Sample location

The samples were collected from the northern part of the Paraná Basin, (in the states of Goiás and Mato Grosso). In this region, the dolostone levels of the Assistência Member (Irati Formation) are exploited in six quarries (Mentel, Império, Ruaro, Metago, Sucal, and Elba) located between the towns of Alto Garças and Montividiu (Figure 1). Some quarry walls exhibit diabase sills (13 m maximum thickness) intruding the sedimentary succession. A set of 27 samples of shales and claystones was selected from various locations and at variable distances from the sills (Figure 2, Table 1). Non-metamorphosed shales were found in sections close to the towns of Alto Garças, Portelândia, Perolândia, and Montividiu. Samples were also collected from sections intruded by diabase sills in the last three localities.

Table 1. Location and lithologies of the samples studied from the quarries and borehole.

Location	Sample	Lithology	Distance from sill
Alto Garças	AG-3	Black shale	No influence
	AG-5	Black shale	No influence
	AG-28	Black shale	No influence
	AG-37	Dark gray shale	No influence
	AG-39	Greenish gray siltstone	No influence
Portelândia	POR-56	Green claystone	No influence
	POR -59	Light green claystone	No influence
	POR-62	Black shale	No influence
	POR-74	Black shale	No influence
	POR-75	Green claystone	No influence
	POR-79	Black shale	3 m
	POR-84	Laminated dark gray claystone	2 m
	POR-88	Laminated greenish gray claystone	In contact
	POR-89	Light green claystone	0.3
Perolândia	(7)	Laminated greenish gray claystone	0.5 m
	(9)	Black shale	1.25 m
	(18)	Laminated green claystone	1 m
	(20)	Gray siltstone	2.5 m
	(44)	Dark gray shale	7.7 m
	(60)	Black shale	In contact
	(66)	Dark gray shale	No influence
	(70)	Dark gray shale	No influence
	MP-229	Black shale	3 m
Montividiu	ELBA-91	Black shale	No influence
	ELBA-93	Black shale	No influence
	FS-1/3	Dark brown shale	4.7 m
	FS-1/9	Black shale	1.5 m
	FS-1/12	Black shale	0.3

https://doi.org/10.1346/CCMN.2010.0580503 Published online by Cambridge University Press

METHODS

The samples were studied by means of X-ray diffraction (XRD), scanning electron microscopy (SEM) with an energy dispersive X-ray spectrometer (EDS), transmission electron microscopy (TEM), and Fourier-transform infrared spectrometry (FTIR). Bulk chemical analyses of major and trace elements, including *REE*, were performed using inductively coupled plasma atomic emission spectroscopy (ICP-AES) and Inductively Coupled Plasma Mass Spectrometry (ICP-MS), respectively.

The XRD patterns were obtained from randomly oriented powders and from oriented preparations. The samples were crushed gently in an agate mortar and then dispersed into distilled water using ultrasonic treatment. The <2 μm fractions were separated by centrifugation. The XRD patterns of oriented preparations and randomly oriented powders were recorded using a PANanalytical Xpert Pro diffractometer equipped with an Xcelerator detector (Ni-filtered CuKα radiation, 40 kV, 40 mA, and step size of 0.017º2θ). The oriented preparations were analyzed in the air-dried state (AD) relative to laboratory ambient humidity (45−55%) and in an ethylene glycol solvated state (EG).

In order to study the variation in the CSDS of smectite and talc particles at different distances from the sills, the full-width at half-maximum (FWHM) of the (001) peaks was measured directly from XRD patterns of Ca-saturated samples in the EG and AD states, respectively. The XRD patterns from randomly oriented powders were decomposed into Gaussian and Lorentzian elementary curves in the 59−63º2θ CuKα angular domain using *DECOMPXR* (Lanson, 1997). Because the background is almost linear in that angular domain, the error due to its subtraction from the XRD patterns was limited. Three groups of trioctahedral phyllosilicates were distinguished according to the following parameters (Bailey, 1980; Brindley, 1980): 1.53 Å or 1.52 Å: (063) reflections for saponite (or saponite-talc mixed-layer minerals) and nontronite, respectively; 1.527 Å and 1.515 Å: (060) and (330) reflections for talc; 1.538 Å and 1.505 Å: (060) and (061,204) reflections for lizardite.

The compositions of mixed-layered structures (saponite/talc or smectite formed of low- and high-charge layers) was estimated roughly by comparison with calculated patterns using *NEWMOD* software (Reynolds, 1985). The heterogeneity of expandable layers was investigated through different ionic saturations (Meunier *et al.*, 2004). Saponite- and nontronite-rich samples were Ca-, K-, and K-Ca-saturated using 1 N solutions of KCl and $CaCl_2$.

Accessory minerals were identified using XRD of randomly oriented powders. The 50−200 μm and 2−50 μm fractions of claystones and shales, respectively, were separated into two parts using dense liquids (bromoform-ethanol mixture with a density, ρ, of 2.72 g/mL). The two subfractions with $\rho < 2.72$ g/mL and $\rho > 2.72$ g/mL were studied in three shale samples not influenced by contact metamorphism.

Observations by SEM of thin sections were performed using a JEOL 5600 LV equipped with EDS (accelerating voltage 15 kV, probe current 2.5 nA, secondary electron and backscattered electron modes). The morphology of clay crystallites in the <2 μm fraction was studied by dispersing this material on a copper grid and then analyzing it using a Philips TEM/STEM Model CM120 equipped with an EDS spectrometer operating at 120 kV.

FTIR spectra in the 4000−250 cm^{-1} range were obtained using a Nicolet 510 spectrometer. The pellets were prepared by mixing 1 mg of sample with 150 mg of KBr and heating overnight at 110ºC to remove any adsorbed water.

Whole-rock major and trace elements were analyzed using ICP-AES and ICP-MS, respectively, in the SARM laboratory (Service d'Analyse des Roches et des Minéraux du CNRS, Nancy, France) in accord with analytical conditions employed in that laboratory (http://www.crpg.cnrs-nancy.fr/SARM). The *REE* patterns were normalized to CI chondrite (Evensen *et al.*, 1978) and compared with the average shales from the PAAS (Taylor and McLennan, 1985) and NASC (Gromet *et al.*, 1984) collections.

RESULTS

Petrographic characteristics

Sedimentary features (unmetamorphosed sedimentary rocks). The black shales are finely laminated and lightly undulated (Figure 3a,b). The claystones are massive to finely laminated. Both rock types consist mainly of Mg,Fe-clay minerals, quartz, micritic calcite-dolomite, and, rarely, feldspar. The clay minerals are oriented parallel to the sedimentary bedding. Quartz grains are moderately sorted (clay-silt fraction) and sub-rounded in the majority of the samples, except in sample POR-56 where they are sub-angular and poorly sorted (Figure 3c).

Metamorphic features (metamorphosed sedimentary rocks). Despite metamorphic mineral reactions, in the meta-shales and meta-claystones the original sedimentary lamination features are preserved. An ostracod-rich meta-black shale and a meta-claystone exhibit albite pseudomorphs of ostracod carapaces (Figure 3d). Next to sills, stylolites and microveins parallel or oblique to the lamination are filled with organic matter, calcite, quartz, pyrite, and pyrolusite (Figure 3e). Metamorphic clay minerals are predominantly randomly oriented (Figures 3f, 4), but sometimes parallel to the lamination (Figure 4). The meta-claystones at 0.7 and 1 m from the sill (samples 7 and 18) present metamorphic 1−20 μm

https://doi.org/10.1346/CCMN.2010.0580503 Published online by Cambridge University Press

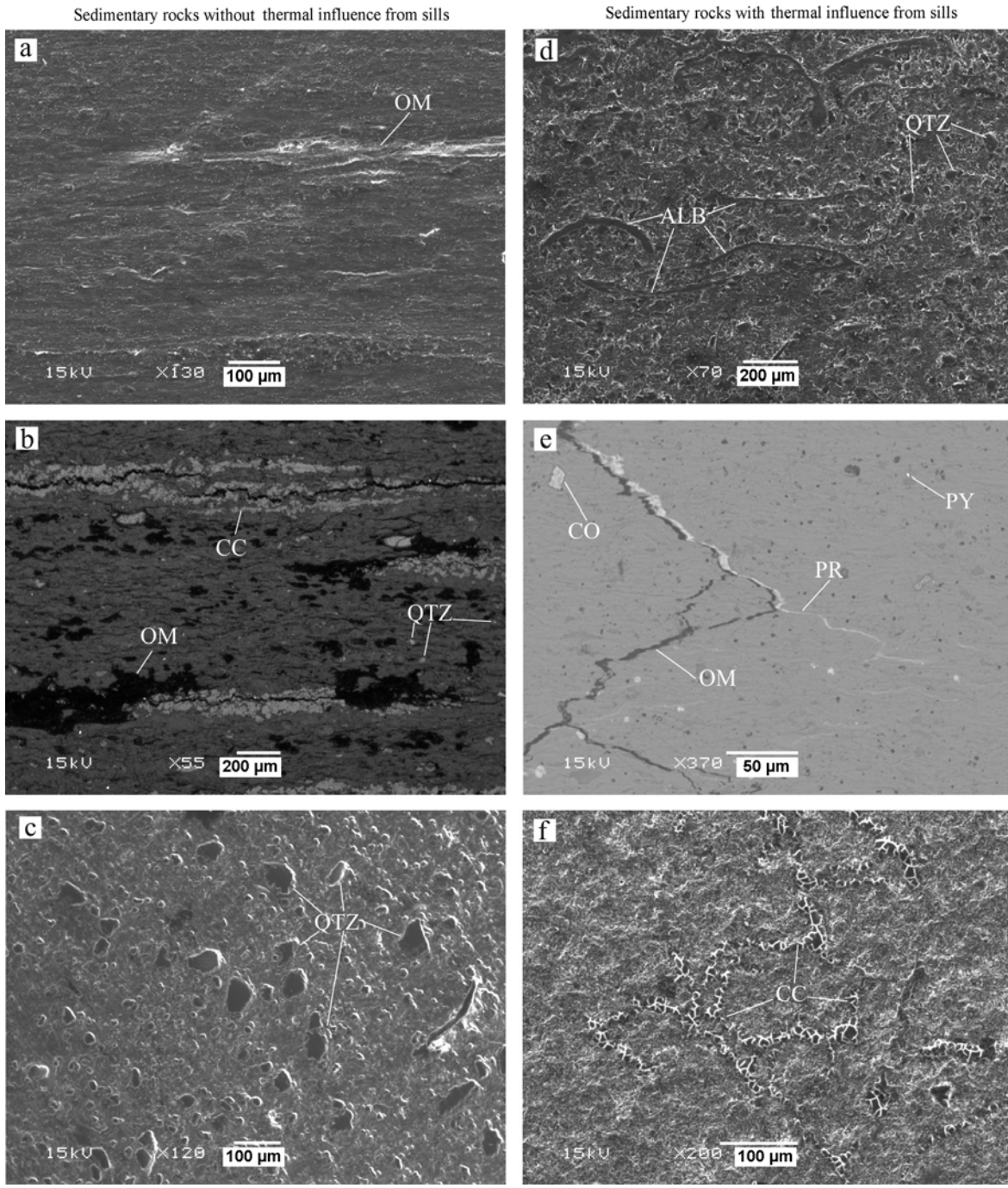

Figure 3. Matrix texture of black shales (a,b) and green claystone (c) without thermal influence caused by the sill; and black shales (d,e) and green claystone (f) with thermal influence caused by the sill. The SEM images perpendicular to the sedimentary bedding were obtained in secondary (SE) and backscattered (BSE) electron modes. (a) Laminated black shale (ELBA-91) consisting of saponite, quartz, calcite, dolomite, and organic matter veins (SE); (b) laminated black shale (POR-74) consisting mainly of saponite, lizardite, talc, and quartz, with organic matter and calcite veins (BSE); (c) massive claystone (sample POR-56) composed mainly of nontronite and quartz, (SE); (d) laminated black shale (MP-229) comprising saponite and quartz with albite pseudomorphs of ostracod carapaces (SE); (e) laminated black shale (60) comprising talc and quartz with organic matter and pyrolusite veins (BSE); (f) massive claystone (18) composed mainly of saponite, lizardite, metamorphic pyroxene, and calcite with a colony of algae (*Pyrrophycophyta*?) of calcitic composition (SE). ALB: albite; CC: calcite; CO: corundum; OM: organic matter; PR: pyrolusite; PY: pyrite; QTZ: quartz.

https://doi.org/10.1346/CCMN.2010.0580503 Published online by Cambridge University Press

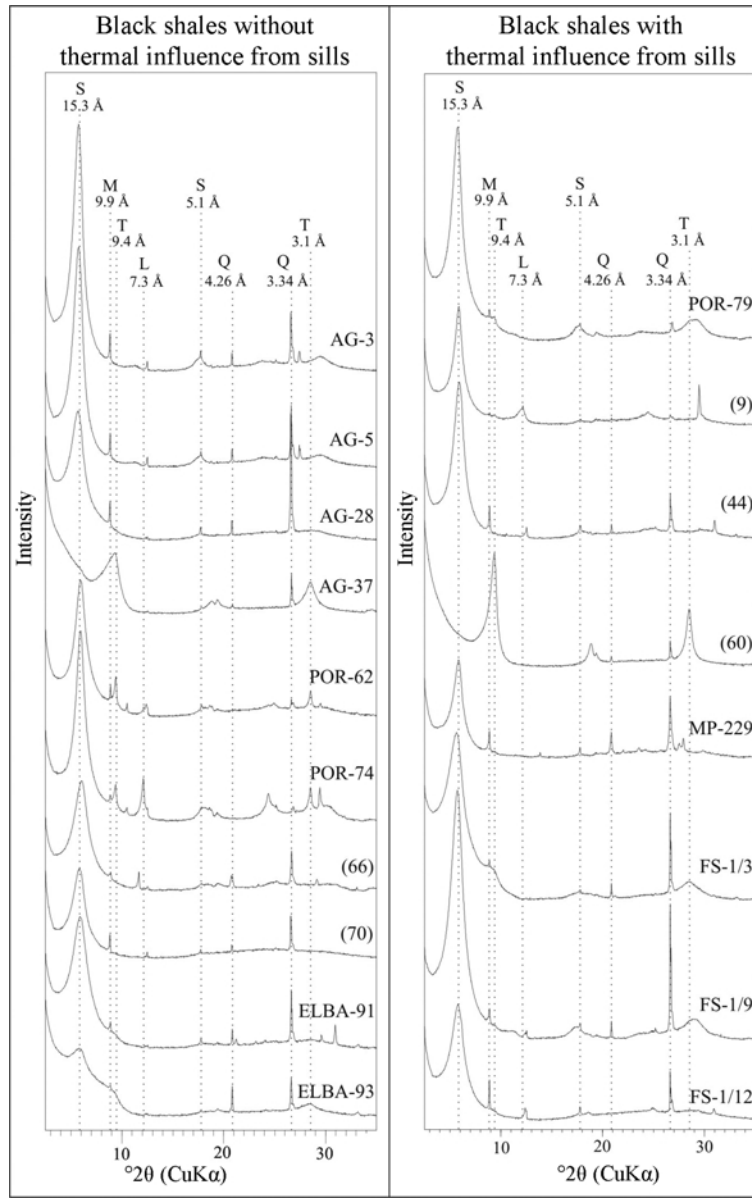

Figure 4. XRD patterns of the <2 μm fraction of the black shales (oriented preparations in the AD state). L: lizardite; M: mica; N: nontronite; Q: quartz; S: saponite; T: talc.

long, euhedral pyroxene crystals (enstatite-augite) dispersed in the matrix (Dos Anjos, 2003).

Accessory minerals. The accessory minerals identified in shales and siltstones are amphibole, pyroxene, hematite, anatase, rutile, badelleyite, spinel, hyttsjoite (Pb-Ba silicate), benitoite, native silver, acanthite, zircon, monazite, apatite, cassiterite, barite, titanite, ilmenite, corundum, garnet, and phengite. The minerals seemed to be distributed homogeneously among the different sedimentary layers. The green claystone from Portelândia (sample POR-56), however, is anomalously rich in zircon and monazite.

Mineralogical composition of the clay fraction

The clay fraction of black shales and green claystones is most often a polyphased assemblage including two or three different species, *e.g.* saponite, nontronite, talc (or talc-rich mixed-layer minerals), and lizardite. Dioctahedral mica and chlorite are detected in trace amounts (chlorite occurs only in three samples from Portelândia). The only monophase sample is POR-56.

Saponite. The trioctahedral smectite was identified by a d_{001} value ranging from 14.9 to 15.5 Å in the AD state, which shifts to 16.8−17.2 Å in the EG state and a d_{060} value of 1.53 Å (Figures 4−7). The XRD patterns of

https://doi.org/10.1346/CCMN.2010.0580503 Published online by Cambridge University Press

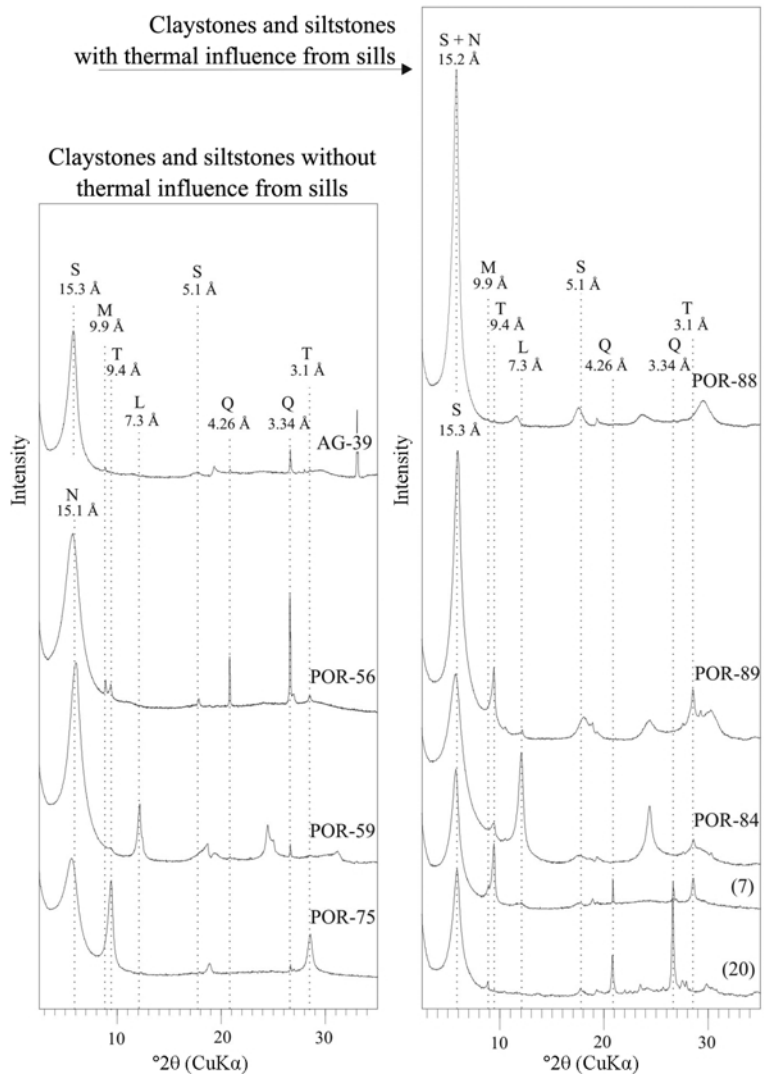

Figure 5. XRD patterns of the <2 μm fraction of claystones (oriented preparations in the AD state). L: lizardite; M: mica; N: nontronite; Q: quartz; S: saponite; T: talc.

samples in the Ca-EG state showed that the (002) peak profile is symmetrical and the d_{002} varies from 8.45 to 8.56 Å. This indicates that the smectite crystallites are composed of fully expandable layers (Reynolds, 1980). The FWHM of the (001) reflection (AD state) varies from 0.7 to 1.2º2θ in samples far from sills while it decreases to 0.6º2θ in thermally metamorphosed rocks (Figure 7a). The 3675 cm^{-1} band (OH-stretching region, Figure 8) indicates the presence of 3Mg-OH groups (Grauby *et al.*, 1994). The smectite crystallites (TEM images) are anhedral and edge rolled (Figure 9a).

Nontronite. The presence of an Fe-rich dioctahedral smectite (nontronite) is indicated by the d_{060} reflection at ~1.52 Å (Figure 6). Its d_{001} reflection is indistinguishable from that of saponite in both AD and EG states (Figures 4–6). Because sample POR-56 is monomineralic, the expandability of the nontronite layers was easier to characterize. The (001) peak at ~15 Å shifted to 16.9 in the Ca-EG state. The expandability was decreased in the K-saturated sample but recovered after Ca-K-saturation. Because the K-saturation had not collapsed the expandable layers irreversibly, the nontronite particles could be considered as being formed of low-charge layers. The broad OH-stretching band between 3558 and 3585 cm^{-1} indicated the presence of $2Fe^{3+}$-OH and Fe^{3+}-Al-OH groups (Figure 8), the absorption bands of which were at 3550 and 3570 cm^{-1}, respectively (Farmer, 1974; Goodman *et al.*, 1976). Some nontronite samples also show a band at 874 cm^{-1} which is typical of Al-Fe^{3+}-OH groups. Nontronite crystallites (TEM images) exhibit a euhedral hexagonal habit from isometric plates to elongated laths (Figure 9b).

https://doi.org/10.1346/CCMN.2010.0580503 Published online by Cambridge University Press

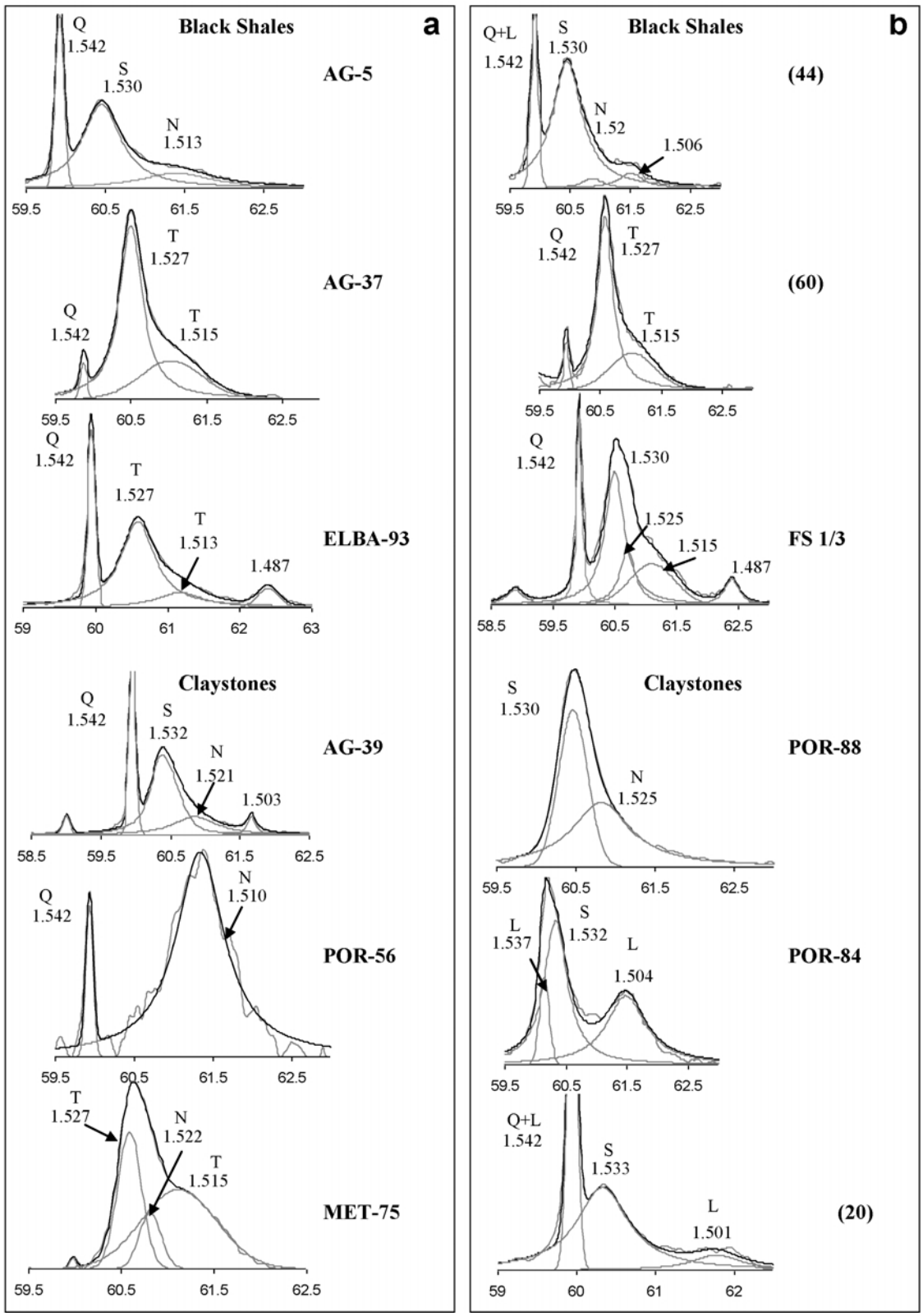

Figure 6. XRD patterns of randomly oriented powder preparations in the 59.5–63°2θ (CuKα) range. Decomposition was carried out using Gaussian curves (Lanson, 1997). L: lizardite; N: nontronite; Q: quartz; S: saponite; T: talc.

https://doi.org/10.1346/CCMN.2010.0580503 Published online by Cambridge University Press

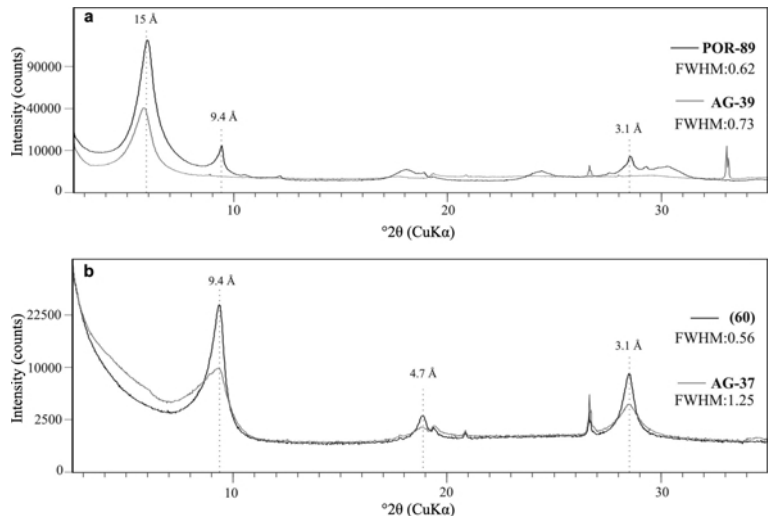

Figure 7. XRD patterns of oriented preparations of the <2 μm fraction in the AD state. Comparison of the full width at half height (FWHM) of the 001 peak for (a) saponite and (b) talc. Samples were selected based on the predominance of these two clay species.

Talc and talc-rich mixed-layer minerals. The presence of talc was characterized by (001), (060), and (330) reflections at 9.33, 1.527, and 1.515 Å, respectively (Figures 4–7). The FWHM of the (001) reflection is 1.25 and 0.56º2θ in the enriched levels far from and in contact with the sill, respectively, indicating an increase in CSDS to thermal metamorphism (Figure 7b). The presence of talc was confirmed by two absorption bands at 3675 cm^{-1} and 3660 cm^{-1} in the IR spectra (Figure 8). The first is more intense than that of saponite. The second is typical of the 2Mg-*R*-OH groups (*R* = transition metals). Synthetic talc, with *R* = Ni, Fe, Zn, or Co, presents a shift of the 2Mg-*R*-OH vibrations in the range 3661–3664 cm^{-1} (Wilkins and Ito, 1967). In natural samples, the shift of the 2Mg-*R*-OH band indicated that Mg is partially replaced by other divalent cations (Petit *et al.*, 2004). Talc crystals present two different morphologies (TEM images); tabular in the unmetamorphosed shale and prismatic in metamorphosed ones (Figure 10c,d).

Randomly ordered saponite-talc mixed-layer minerals (S-T) are present in some samples such as ELBA-93 and POR-75. The saponite-talc mixed-layer minerals are characterized by: (1) a d_{001} reflection shifting from 15.3 to 17.4 – 17.7 Å in AD and EG states, respectively; (2) a large saddle/peak ratio in the low-angle domain (EG state); and (3) a d_{002} reflection ranging between 8.50 and 9.33 Å in the EG state (Figure 10). Simulations by *NEWMOD* showed that the position and peak profiles of the ELBA-93 and POR-75 samples were reproduced acceptably using a unique talc-rich S-T composition (60% talc layers, 40% saponite layers, $N = 3–7$, S_{40}-T_{60}) mixed with different amounts of saponite ($N = 3–10$) rather than a single S-T in which the relative amounts of saponite and talc layers is variable. In spite of the fact that the procedure based on comparison with *NEWMOD* simulations gives only approximate compositions, the mixture solution seems to be the most acceptable as the S-T composition was consistent with the ELBA 93 and MET-75 samples. The MET-75 samples consist of 100% S_{40}–T_{60} and a mixture of 60% of S_{40}–T_{60} with 40% of saponite, respectively. That the d_{060} reflection of S-T is similar to that of pure talc (Figure 6), in spite of the presence of saponite layers, is remarkable. This is also the case for corrensite in which the d_{060} reflection is similar to that of chlorite (Beaufort and Meunier, 1994).

Lizardite. Lizardite has been detected, using XRD, by means of the (001), (060), and (061, 204) peaks at 7.27, 1.538, and 1.505 Å, respectively. The IR spectra present absorption bands in the 3685–3693 cm^{-1} range and at 670 cm^{-1} and 605 cm^{-1}.

Mica-illite. Mica-illite was identified in the XRD patterns by (00*l*) reflections at 9.9–10.0, 4.99, and 3.31 Å. One crystal of mica or illite was observed, using TEM, in a nontronite-rich claystone (Figure 9e). The elongate crystal had rounded edges, indicating dissolution.

Chlorite. Some XRD patterns contained very low-intensity peaks at 14.2, 7.1, and 4.75 Å, typical of Mg-rich chlorite 00*l* reflections.

Chemical composition

Matrix. Chemical micro-analyses of the shale and claystone matrices at different distances from the sill were plotted on an M^+-4Si-3Mg ternary diagram where M^+ represents the sum of the Na^+, K^+, and $2Ca^{2+}$ ions and 4Si and 3Mg are the amounts of Si^{4+} and Mg^{2+} divided by 4 and 3, respectively (Figure 11). Because of the small crystal sizes, most of the micro-analyses did not plot in the composition field of a single mineral species but

https://doi.org/10.1346/CCMN.2010.0580503 Published online by Cambridge University Press

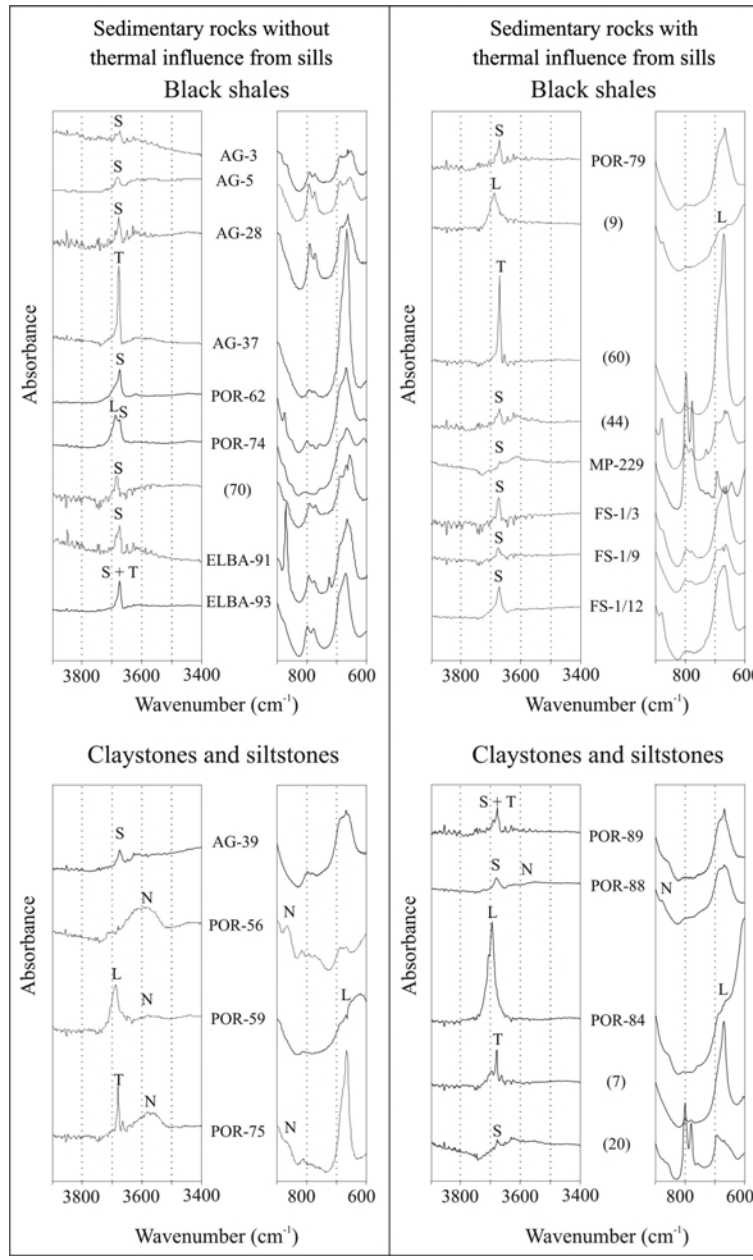

Figure 8. FTIR spectra of the <2 μm fraction of some black shales and claystones far from (a) and near (b) the thermal metamorphic zones of the sills. L: lizardite; N: nontronite; S: saponite; T: talc.

rather in that of bi-phase (mixing lines) or tri-phase (sub-triangles) mineral assemblages. Single-phase compositions of talc, lizardite, saponite, albite, and calcite are located at the intersections of mixing lines or mixing lines with triangle sides. The different tri-phased assemblages are consistent with XRD data and SEM observations. This is particularly important when the composition sub-triangles in the M^{+}-4Si-3Mg coordinates are overlapping as is the case for the saponite-quartz-calcite, saponite-lizardite-calcite, nontronite-quartz-talc, and saponite-quartz-albite assemblages.

Whole rock. Bulk-rock chemical compositions (Table 2) revealed that, except for sample POR-56, all black shales and claystones of the series studied exhibited a MgO-rich composition varying from 11.67 to 30.74 wt.%. All these samples have a clay fraction dominated by trioctahedral magnesian clay species (saponite, talc, lizardite). Two samples are Ca-rich (6 and 7 wt.%) because of the presence of carbonates (calcite and dolomite). The POR-56 sample is Fe_2O_3- and Al_2O_3-rich and MgO-poor compared to the other rocks. This is consistent with the predominance of nontronite in the clay assemblage.

https://doi.org/10.1346/CCMN.2010.0580503 Published online by Cambridge University Press

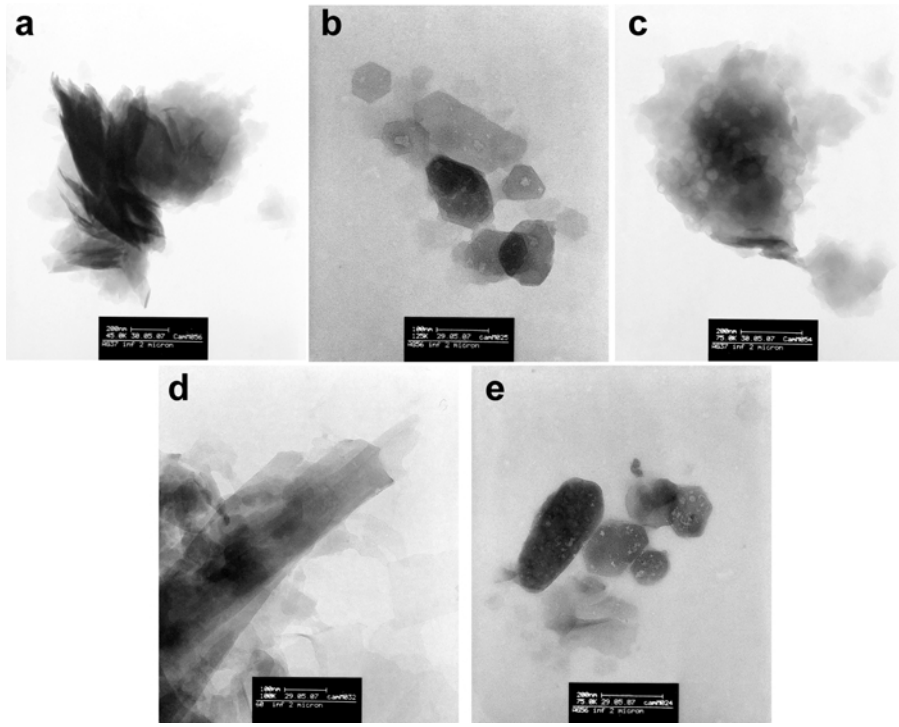

Figure 9. TEM images showing the morphology of the clays: (a) anhedral saponite crystallites with rolled edges (70); (b) euhedral hexagonal nontronite crystallites from isometric plates to elongated laths (POR-56); (c) tabular crystallites of talc in unmetamorphosed black shale (AG-37); (d) prismatic talc crystallites in metamorphosed black shale (60); (e) euhedral, hexagonal nontronite crystallites with an elongated illite crystallite exhibiting rounded edges and dissolution features (POR-56).

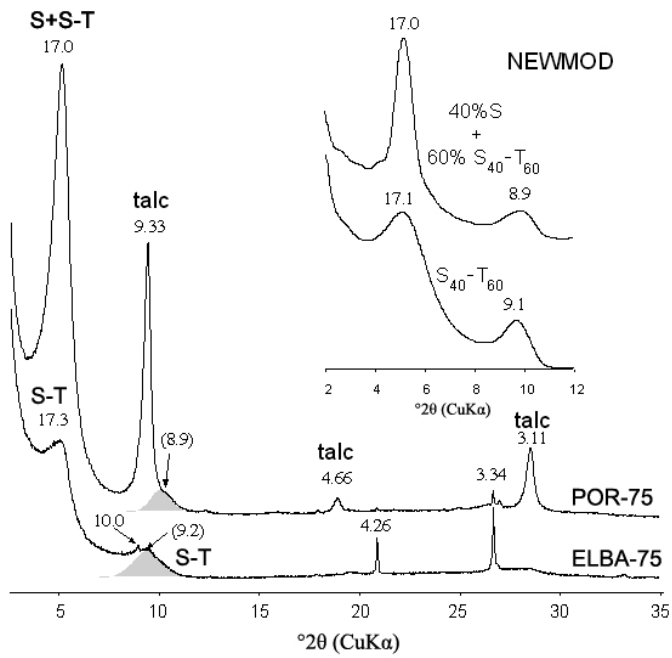

Figure 10. The presence of randomly ordered saponite-talc mixed-layer minerals. The interpretation of experimental XRD patterns was conducted by comparison with calculated patterns using *NEWMOD* (Reynolds, 1985) (oriented preparations in the EG-solvated state of the <2 μm fraction of claystones (POR-75) and black shale (ELBA-93)). Numbers in brackets indicate approximately the apex of the 002 diffraction band (gray area).

https://doi.org/10.1346/CCMN.2010.0580503 Published online by Cambridge University Press

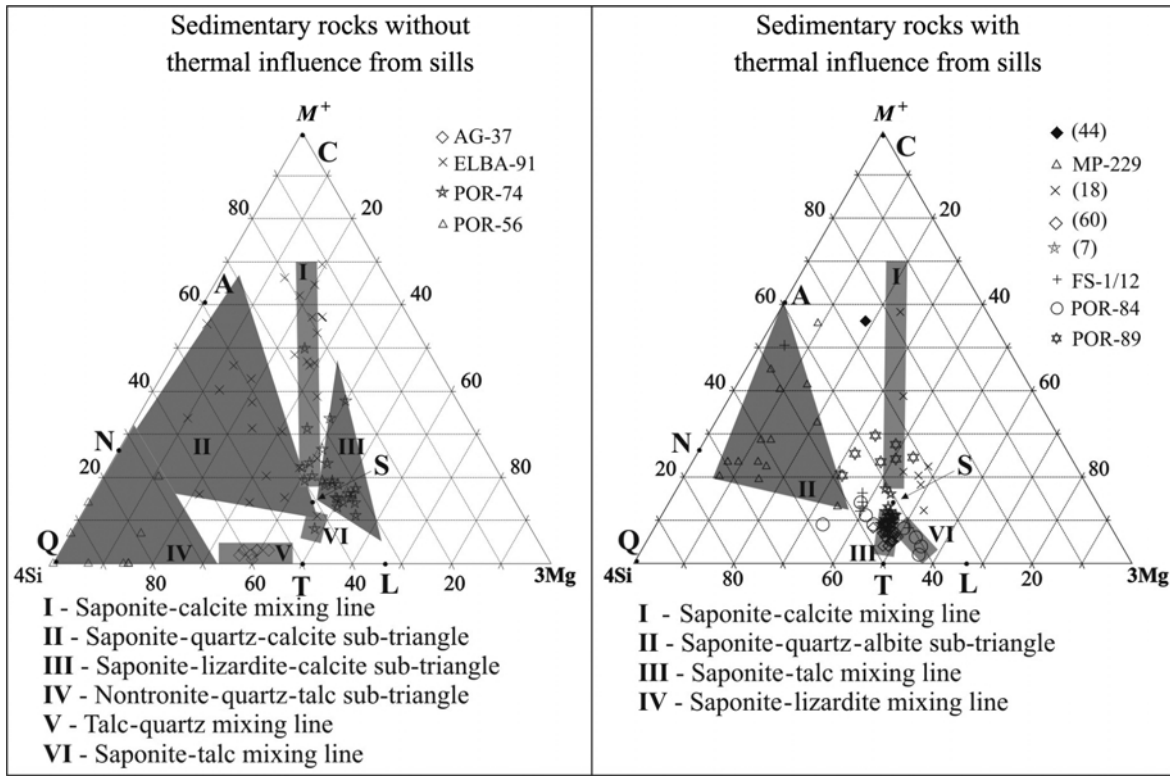

Figure 11. Projection in the M^+-4Si-3Mg diagram of SEM/EDS micro-chemical analyses of the clay matrix. The analyzed samples were black shales and claystones (a) far from and (b) within the sill thermal-metamorphic zones. A: albite, C: calcite, L: lizardite, N: nontronite, S: saponite, Q: quartz, T: talc.

With the exception of the nontronite-rich claystone (sample POR-56), which is geochemically different from the other samples, the TiO_2, Cr, and P_2O_5 contents are positively correlated with Al_2O_3 (Figure 12). A similar trend is observed in weathered profiles developed on basic or ultrabasic rocks, where the less-soluble elements are systematically concentrated in altered horizons even if they are present in small amounts in the parent rock (Traoré *et al.*, 2008). This is why bauxite deposits may form on basic and ultrabasic rocks (Tardy, 1997). The CI-normalized *REE* patterns reveal that the clayey rocks are systematically enriched in light *REE* (*LREE*) relative to heavy *REE* (*HREE*) with a negative Eu anomaly. The shape of all the patterns was similar to that of PAAS and NASC specimens. Three groups can be distinguished (Figure 13): (1) *REE*-enriched rock relative to PAAS and NASC with a large negative Ce anomaly (POR-56 claystone); (2) black shales and claystones with *REE* content close to PAAS and NASC specimens; or (3) depleted compared to PAAS and NASC specimens. The *REE* content of these clayey rocks can be correlated with their dominant clay assemblages: talc-saponite with the depleted rocks; saponite-lizardite-nontronite with rocks close to PAAS and NASC; and nontronite with large *REE* contents (POR-56). Black shales and claystones are indistinguishable in the two former groups. Small *REE* concentrations relative to PAAS and NASC are typical of Mg-rich clay minerals formed either from the weathering of ultramafic rocks (Dampare *et al.*, 2005) or precipitated in an alkaline lake environment (Furquim *et al.*, 2008). Nevertheless, a difference was observed in the Ce and Eu anomalies which are positive in the lacustrine environment and negative in the weathered rocks. The black shales and claystones studied here exhibit a negative anomaly.

DISCUSSION

The rocks of the Irati Formation, prior to the intrusion of Cretaceous diabase sill, failed to attain temperatures of >80ºC (Araújo *et al.*, 1996). Even if little is known about the kinetics of Mg-rich trioctahedral smectites in natural systems, such temperatures are unlikely to lead to the disappearance of saponite (Whitney, 1983). The clay-mineral assemblages forming the black shales and the claystones could, therefore, have preserved some of their depositional signature. Most of the mineralogical modifications observed in the rocks sampled close to the sills may be attributed to the thermal metamorphism aureole.

https://doi.org/10.1346/CCMN.2010.0580503 Published online by Cambridge University Press

Table 2. Chemical composition (major and trace elements) of representative samples of black shales and claystones located away from the thermal metamorphic zones caused by sills.

Major oxides	Black shales					Green silt- and claystones			
(wt.%)	AG-28	AG-37	ELBA-91	ELBA-93	POR-74	70	AG-39	POR-56	POR-59
SiO_2	61.21	60.79	44.20	64.31	48.19	55.68	75.60	53.63	45.43
Al_2O_3	3.66	0.96	2.56	2.03	3.89	3.85	2.90	13.40	4.66
Fe_2O_3	3.00	2.66	4.15	5.18	1.09	2.66	3.60	18.58	5.00
MnO	0.01	0.01	0.14	0.02	0.10	0.06	0.02	0.03	0.33
MgO	21.55	28.19	22.84	19.23	26.80	22.88	11.67	4.24	30.74
CaO	1.88	0.24	7.13	0.99	5.98	0.57	0.34	0.14	0.45
Na_2O	0.08	0.08	< D.L.	< D.L.	0.20	< D.L.	< D.L.	< D.L.	0.09
K_2O	0.32	0.07	0.19	0.19	0.22	0.33	0.24	< D.L.	< D.L.
TiO_2	0.20	0.05	0.13	0.13	0.26	0.24	0.22	0.40	0.26
P_2O_5	0.08	0.02	0.04	0.04	0.17	0.13	0.05	0.09	0.15
LOI	7.94	6.98	18.84	7.10	12.56	13.23	4.27	10.30	11.66
Sum	99.94	100.05	100.21	99.21	99.45	99.62	98.91	100.79	98.78
Trace elements and *REE* (ppm)									
Ce	13.630	12.040	16.480	11.260	83.500	39.220	17.410	58.470	21.500
Cr	17.590	4.841	13.190	12.540	28.610	19.850	17.090	61.160	28.380
Dy	1.040	0.652	1.379	0.827	4.844	3.543	1.256	41.220	3.355
Er	0.534	0.339	0.825	0.432	2.988	1.830	0.751	21.430	1.888
Eu	0.292	0.175	0.325	0.195	0.983	0.888	0.286	11.590	0.857
Gd	1.278	0.835	1.557	1.010	5.453	4.424	1.433	46.170	4.039
Ho	0.199	0.126	0.300	0.154	0.967	0.686	0.259	8.051	0.690
La	9.208	9.858	9.891	6.512	34.520	22.900	9.377	229.000	22.950
Lu	0.084	0.046	0.121	0.064	0.608	0.238	0.134	2.778	0.258
Nb	5.031	1.165	2.802	2.705	7.033	5.336	4.694	8.677	5.744
Nd	7.380	5.282	8.120	5.727	31.160	20.590	8.276	204.200	18.640
Pr	1.851	1.379	2.013	1.424	7.878	4.912	2.125	48.540	4.514
Sm	1.455	0.934	1.657	1.149	6.218	4.517	1.707	43.790	3.872
Tb	0.187	0.118	0.227	0.147	0.821	0.639	0.222	7.103	0.567
Tm	0.077	0.047	0.117	0.060	0.483	0.243	0.115	2.966	0.254
Y	6.790	4.519	9.920	5.212	31.410	22.850	7.376	272.600	28.690
Yb	0.527	0.293	0.754	0.409	3.628	1.552	0.826	18.230	1.590
Zr	91.930	25.190	39.400	73.210	164.400	98.080	245.600	181.900	94.690

Origin of the Mg-,Fe-rich clay minerals

The clay mineral assemblages of shales and siltstones from unmetamorphosed and metamorphosed zones (Table 3) are consistent with the formation of Mg-smectites, which is known to be favored in three different geological contexts: (1) evaporative basins (Hover *et al.*, 1999; Bristow *et al.*, 2009); (2) weathered mafic-ultramafic rocks; and (3) hydrothermal settings (see Meunier, 2005, for a review). The chemical conditions (pH and salinity) in evaporative systems also favor the precipitation of salts such as gypsum and the formation of zeolites from volcanic ashes or detrital silicates (Chamley, 1989). Several other Mg-clay minerals, especially sepiolite, palygorskite, stevensite, and, more rarely, talc, may crystallize in such alkaline and saline conditions either by direct precipitation from solution, by conversion of dolomite, or by topotactic overgrowth on pre-existing phyllosilicate templates (April, 1981; Khoury *et al.*, 1982; Rehim *et al.*, 1986; Akbulut and Kadir, 2003; Cuevas *et al.*, 2003; Karakaya *et al.*, 2004).

The salinity of the Irati Formation varied from normal to hypersaline (Sanford and Lange, 1960; Rodrigues and Quadros, 1976; Santos Neto, 1993). Some cm-thick levels of gypsum and nodular anhydrite in dolomite mudstone occur in the northeastern part of the basin (Santos Neto, 1993). Dos Anjos (2003) described sepiolite as a trace mineral in the dolomite mudstones of the Irati Formation. Neither sepiolite nor minerals typical of evaporitic systems have been found in the black shales or the interbedded claystones. Therefore, assigning an authigenic origin to the traces of sepiolite detected in the dolomite-mudstones is impossible. The sepiolite could be due to eolian contamination. The occurrence of gypsum and anhydrite is limited to the northeastern part of the basin but the quantities are too small to suggest that evaporitic conditions were established during the time of their deposition.

The alternative is to consider that the clays forming shales and claystones originated from eroded, weathered mantle minerals developed on partially or totally serpentinized basic- to ultrabasic rocks. The presence of nontronite, talc, and lizardite, even in small amounts,

https://doi.org/10.1346/CCMN.2010.0580503 Published online by Cambridge University Press

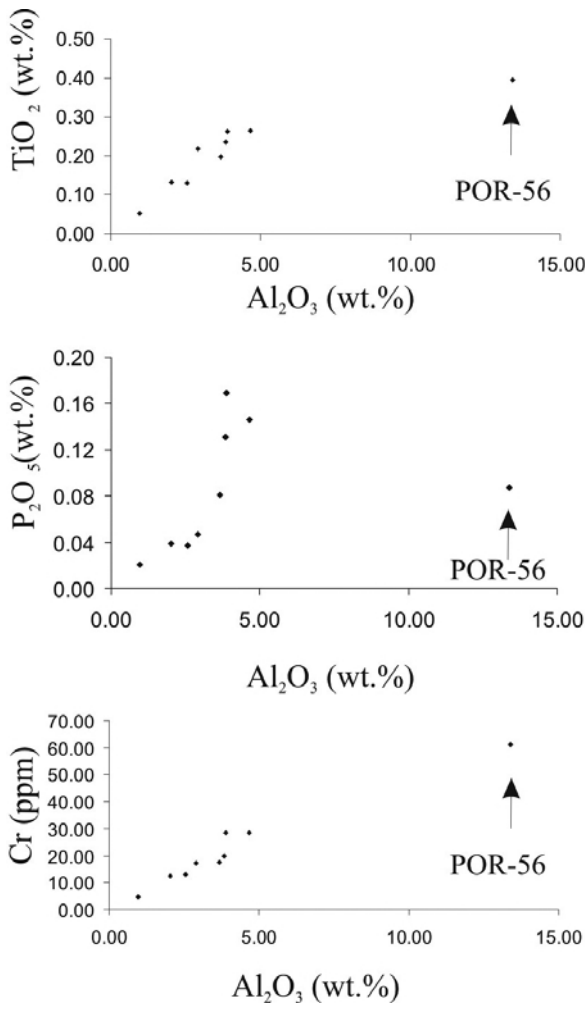

Figure 12. Variation of the TiO_2 (wt.%), P_2O_5 (wt.%), and Cr (ppm) amounts *vs*. Al_2O_3 (wt.%) of black shales and green claystones.

in some shale samples, implies a detrital source because they are ordinarily associated with saponite in the alteration products of pyroxene, olivine, serpentine, or amphibole (Eggleton and Boland, 1982; Nahon *et al.*, 1982; Fontanaud and Meunier, 1983; Noack and Duplay, 1983; Colin *et al.*, 1990; Noack *et al.*, 1993; Sakharov *et al.*, 2004; Yalçin and Bozkaya, 2006). The presence of mafic detrital silicates (amphibole, pyroxene) and chromium spinel in the black shales and claystones of the Irati Formation on one hand, and the absence of detrital alkali- and Al-rich clay minerals on the other hand, indicate weathered mafic/ultramafic rocks as sediment sources. This is supported by the negative Ce and Eu anomalies (Figure 12) and the correlation of the TiO_2, Cr, and P_2O_5 amounts with Al_2O_3 (Figure 11). The *REE* contents are systematically less than in PAAS-NASC specimens, indicating that the sedimentation environment has not significantly modified the inherited composition.

The absence of clay minerals formed in weathered granitic rocks such as kaolinite and dioctahedral Al-rich clay minerals suggests that these rocks were not exposed in the catchment supplying sediments to the northern part of the basin during the deposition of the Irati Formation.

Possible sediment sources could include the pyroxenite, amphibolite, serpentinite, talc schist, and metabasalts located in the northern border of the Paraná basin. All these rock types are present in the metavolcano-sedimentary sequences of the Neoproterozoic Goiás Magmatic Arc, which is tectonically separated by mylonitized orthogneisses of dioritic to granitic composition (Dardenne, 2000).

If mafic-ultramafic rocks are considered to be the source of the Mg- and Fe-clay minerals forming the black shales and claystones in the sedimentary series, the POR-56 green claystone must be considered separately. In the POR-56 sample, euhedral zircon, monazite, and apatite are more abundant than in the other samples, suggesting that volcanic ash was the precursor material and explains the enriched *REE* pattern (Figure 13). The strong negative Ce anomaly indicates an interaction between saline water and volcanic ash (Piper, 1974; Desprairies and Bonnot-Courtois, 1980). The question then becomes why nontronite formed instead of Al-smectites as is usually the case in bentonite deposits?

Several tuff, bentonite, or tonstein beds have been described in the Carboniferous and Permian units of the Gondwana basins. The Permian units of the southern part of the Paraná Basin (Irati, Rio Bonito, and Yaguari Formations) exhibit several-cm thick bentonite and tonstein layers (Coutinho *et al.*, 1988; Maynard, 1996; Matos *et al.*, 2001; Calarge *et al.*, 2003, 2006; Coutinho and Hachiro, 2005; Santos *et al.*, 2006). The chemical analyses of these levels show that they derived from rhyolitic ash (Figure 14). The probable source of the ash was the Choiyoi Province (Figure 15), a calc-alkaline magmatic arc developed between 275 and 250 Ma in southern Gondwana (Kay *et al.*, 1989). Intermediate to mafic ash-fall layers have also been described in the Gondwana basins. Some trachyandesitic bentonite layers were reported in the Carboniferous Juruá Formation in the Solimões basin, northern Brazil (Alves and Vaz, 2006), and in the Permian Beauford Group in the Karoo basin, South Africa (Keyser and Zawada, 1988). Basaltic/andesitic tuff beds occur in the Permian Prince Albert Formation in the Main Karoo basin, South Africa (McLachlan and Jonker, 1990; Stollhofen *et al.*, 2000).

According to the geochemical classification of Winchester and Floyd (1977), the nontronite-rich bed could derive from andesitic ash and not from rhyolitic ones as is the case in the south of the basin (Figure 13). Those types of ash could react with sea water giving nontronite (Hein and Scholl, 1978; Kastner, 1999). Consequently, the volcanic sources of the ash in the Irati formation of the northern part of the Paraná basin

https://doi.org/10.1346/CCMN.2010.0580503 Published online by Cambridge University Press

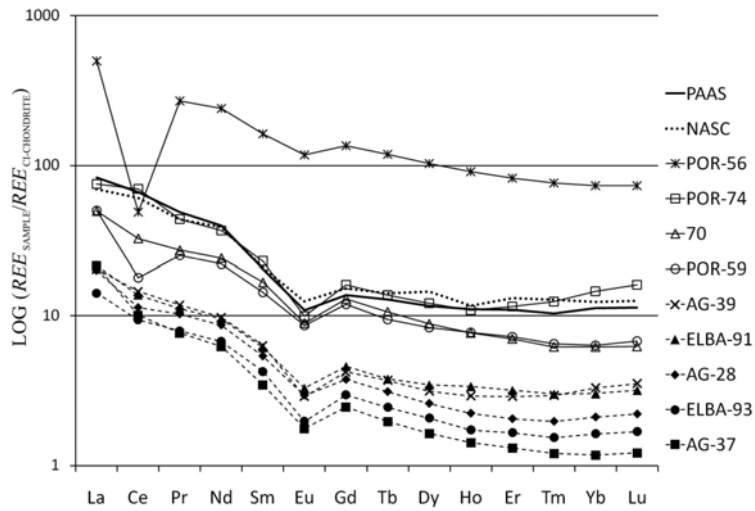

Figure 13. CI-normalized *REE* patterns of black shales (AG-28, AG-37, ELBA-93, POR-74, 70) and claystones (AG-39, POR-56, POR-59) without thermal influence caused by sills. CI-normalized *REE* patterns of PAAS and NASC specimens are also shown.

were different from those which were active in the southern part. The Mitu volcanic area in the Central Andes is a possible alternative source for the ash forming the nontronite-rich bed (Figure 15). Indeed, this area is mainly formed of alkaline basalts with subordinate tholeiitic basalts, dacites, and rhyolites. The volcanism is related to the extensional tectonics which affected this area during the interval between the pre-Andean ('late Hercynian') and Andean orogenies (Kontak *et al.*, 1990). The isotopic ages of Mitu volcanic activity near Lake Titicaca in Peru (280–260 Ma) permits a possible contribution to sediments in the Irati formation (Sempere *et al.*, 2002).

Effect of thermal metamorphism on the clay minerals

Saponite and talc were observed at a range of distances from the sills and significant differences in crystallinity, texture, and relative quantity were observed. The FWHM of their 001 XRD peak decreases near the sills, indicating that their CSDS increases. Furthermore, saponite and talc particles were randomly oriented in the metamorphosed zone as observed using SEM. This implies post-depositional crystal growth. Concomitantly, the nontronite observed in the green claystones far from sills disappeared progressively while saponite became dominant.

Saponite is stable under high-temperature conditions. Bouchet *et al.* (1992) showed that the Mg-rich smectite formed after heating at 175ºC for 4 y in a bentonite barrier made of a mixed-layer kaolinite-smectite clay material. Abad *et al.* (2003) showed that saponite formed in thermally metamorphosed marly rocks from the Betic Cordilleras, Spain; the marl at 18–20 m from the sill contains saponite + regular chlorite-saponite mixed-layer (corrensite) + beidellitic smectites. Saponite + pyroxene + zeolites and garnet + saponite metamorphic assemblages were observed in mudstones and limestones, respectively, in the Isle of Skye (western Scotland) in the vicinity of an intruding Tertiary sill (Kemp *et al.*, 2005).

In summary, the metamorphosed clayey rocks of the Irati Formation near the sills contain talc, lizardite, pyroxene, and albite. These metamorphic minerals are distinguished from detrital minerals according to their CSDS values, relative quantities, and texture. The metamorphic minerals are parallel to the bedding in

Table 3. Clay minerals forming the sedimentary rocks of the Irati Formation.

	Lithology	Clay minerals
Unmetamorphosed sedimentary rocks	Dark gray to black shales	Saponite, talc
	Greenish gray to green claystone and siltstone layers	Nontronite, lizardite
Metamorphosed sedimentary rocks	Dark gray to black meta-shales	Saponite, talc, lizardite
	Gray to green meta-claystones and meta-siltstones layers	Saponite, nontronite, lizardite

https://doi.org/10.1346/CCMN.2010.0580503 Published online by Cambridge University Press

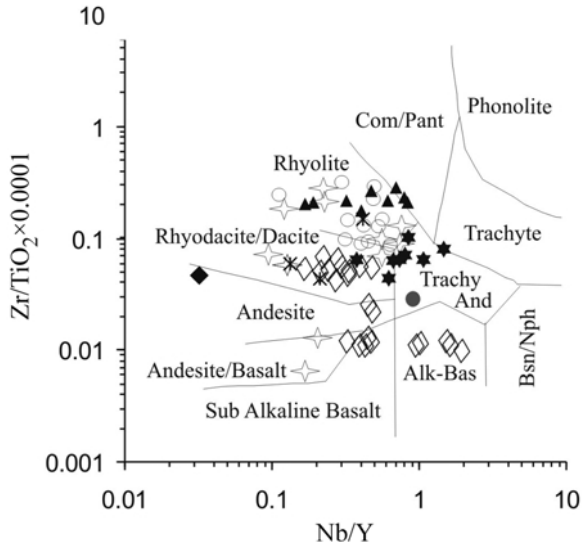

Figure 14. Position of the nontronite-rich claystone (POR-56) in the geochemical classification of Winchester and Floyd (1977). The composition of other volcanic ash deposits are plotted for comparison. *Paraná basin*: POR-56 green bed, Irati Formation (◆); bentonite, southern part (Maynard *et al.*, 1996), Irati formation (✳); and Melo bentonite, southern part (Calarge *et al.*, 2006), Permian Yagari formation (▲). *Solimões basin*: Carboniferous bentonite (Alves and Vaz, 2006), Juruà Formation (✸). *Karoo basins*: fallout tuffs, Permian Collingharn Formation (Viljoen, 1995), *Main Karoo basin* (○); fallout tuff, Permian Prince Albert Formation (McLachlan and Jonker, 1990; Viljoen, 1995), *Main Karoo Basin* (✧); ash-flow tuff, Permian Beauford Group (Keyser and Zawada, 1988), Main Karoo Basin (●); bentonitic tuff beds, Carboniferous –Permian Dwyka Group (Bangert *et al.*, 1999), southern Namibia (◇).

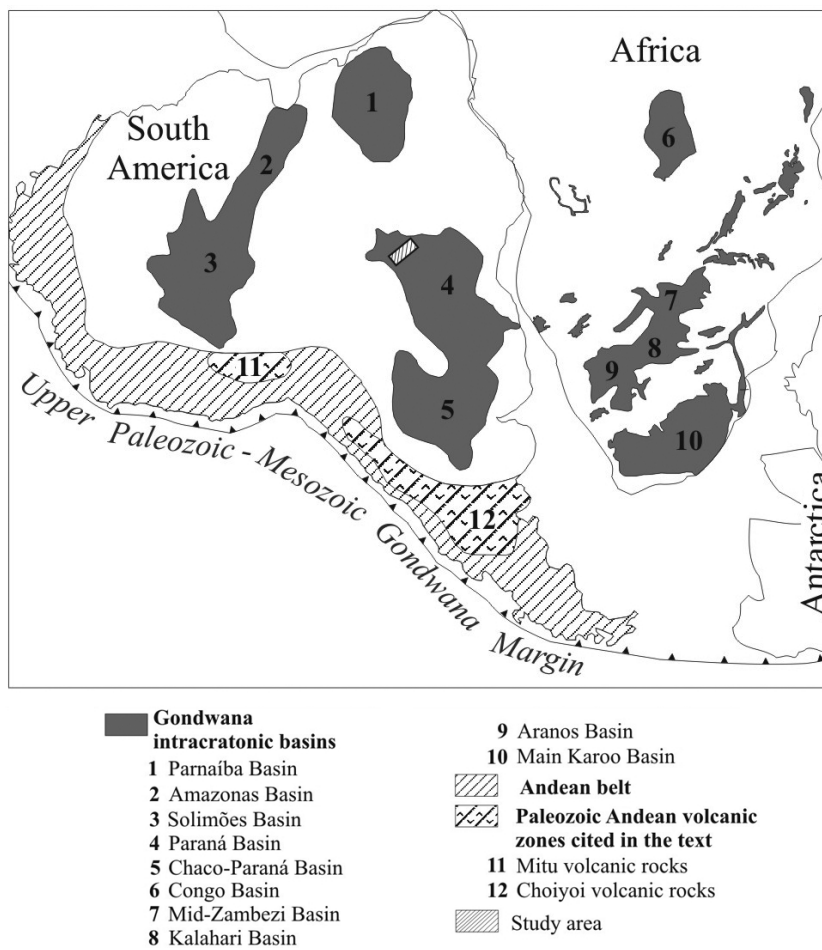

Figure 15. Simplified map of southwestern Gondwana with the location of major intracratonic basins and Andean Volcanic zones cited in the text (based on De Wit *et al.*, 1988; Milani and Thomaz Filho, 2000; Ramos, 2000; Sempere *et al.*, 2002; Catuneanu *et al.*, 2005).

https://doi.org/10.1346/CCMN.2010.0580503 Published online by Cambridge University Press

the unmetamorphosed rocks but become major components in some layers near the sill where they are randomly oriented with respect to the bedding. Pyroxene crystals (1–20 μm) are observed in the matrix of the claystones at 0.7 to 1 m from the sill. Concomitantly, the calcite ostracod carapace is pseudomorphed into albite (Almeida and Do Carmo, 2005). Albite occurs in both black shales and claystones but metamorphic pyroxene crystals were found only in claystones (Dos Anjos, 2003). Lizardite occurs either as detrital grains far from the sill or as a metamorphic mineral next to sills. In the Sucal quarry, the amount of lizardite increased systematically toward the sill (Dos Anjos, 2003). Amphibole always occurs here as a trace mineral with no evidence of metamorphic origin.

The metamorphic generation of clay and non-clay minerals was driven by chemical diffusion inside the sedimentary rocks. No evidence was found for the transfer of chemical components from the sill to the host rocks. The formation of hydrated silicates (saponite, talc, lizardite) points to a large partial pressure for water, which indicates that the chemical system was nearly closed. This does not exclude pyroxene (an anhydrous phase) which has been shown to crystallize with smectites at 200ºC (Decarreau *et al.*, 2004).

CONCLUSIONS

Based on the mineralogical and chemical compositions of black shales and claystones of the Irati Formation, the unusual saponite + nontronite ± talc ± lizardite ± chlorite assemblage probably originated from the dismantling of weathered mafic-ultramafic rocks rather than from precipitation in an evaporative sea environment. The black shale or claystone, marl or limestone alternation, which characterizes the stratigraphical organization of the Irati series, corresponds to weathering/erosion cycles of the neighboring, emerged basement.

Because of its particular trace elements and *REE* composition, the POR-56 claystone cannot be attributed to a detrital origin. Its clay assemblage is monophasic, as are most of the bentonite beds. The unusual abundance of euhedral zircon and monazite crystals indicates a volcanic origin. If this is the case, the nontronite was not inherited from weathered mafic-ultramafic rocks but rather was formed by reaction of glassy ash with sea water. The most likely volcanic episode (lava composition, age, and location) corresponds to the Mitu group (Central Andes).

Except for the POR-56 nontronite bed, the black-shales and claystones are consistently MgO-rich and Al_2O_3-poor. Consequently, the thermal metamorphism induced by the intrusion of diabase sills during the early Cretaceous led to the recrystallization of inherited Mg-rich clay minerals (saponite, talc, lizardite) and the formation of enstatite-augite pyroxenes. The nontronite disappeared, showing that it is unstable in such thermally active, Mg-rich environments.

The present study found that the Paraná basin experienced significantly different sedimentary and diagenetic events in its northern and southern parts and that the geological history of this large, intra-cratonic basin is complex. Extrapolations for the extent of reservoirs must be made cautiously.

ACKNOWLEDGMENTS

The first author acknowledges financial support from the Brazilian agency CNPq – Conselho Nacional de Desenvolvimento Científico e Tecnológico (grants 140869/2004-2 and 202369/2006-4). The authors are grateful to the Mentel, Império, Ruaro, Metago, Sucal, and Elba quarries for providing samples. Sabine Petit is thanked for her help in the interpretation of the FTIR patterns.

REFERENCES

Abad, I., Jiménez-Millán, J., Molina, J.M., Nieto, F., and Vera, J.A. (2003) Anomalous reverse zoning of saponite and corrensite caused by contact metamorphism and hydrothermal alteration of marly rocks associated with subvolcanic bodies. *Clays and Clay Minerals*, **51**, 543–554.

Almeida, C.M. and Do Carmo, D.A. (2005) Taxonomy and palaeoecology of Permian ostracods from the Paraná basin, Goiás State, Brazil. Pp. 11 in: *International Symposium on Ostracoda*, 15, Abstracts.

Almeida, F.F.M., Hasuy, Y., Neves, B.B.B., and Fuck, R.A. (1981) Brazilian structural provinces: an introduction. *Earth Sciences Review*, **17**, 1–29.

Alves, D.B. and Vaz, P.T. (2006) ''Folhelhos verdes'' Carboníferos da Bacia do Solimões: cinzas vulcânicas (K-bentonitas). *Boletim de Geociências da Petrobrás*, **14**, 171–176.

Amaral, S.E. (1970) Geologia e petrologia da Formação Irati (Permiano) no Estado de São Paulo. *Boletim do Instituto de Geociências e Astronomia da USP*, **2**, 8–81.

April, R.H. (1981) Trioctahedral smectite and interstratified chlorite/smectite in Jurassic strata of the Connecticut Valley. *Clays and Clay Minerals*, **29**, 31–39.

Araújo, L.M., Trigüis, J.A., and Cerqueira, J.R. (1996) Avaliação do efeito térmico das intrusivas ígneas nas rochas geradoras da Formação Irati/ Membro Assistência. PETROBRAS/E&P/NEXPAR, Relatório Interno, Curitiba, Brazil, 139 pp.

Bailey, S.W. (1980) Structures of layer silicates. Pp. 2–113 in: *Crystal Structures of Clay Minerals and their X-ray Identification* (G.W. Brindley and G. Brown, editors). Monograph **5**, Mineralogical Society, London.

Bangert, B., Stollhofen, H., Lorenz, V., and Armstrong, R. (1999) The geochronology and significance of ash-fall tuffs in the glaciogenic Carboniferous-Permian Dwyka Group of Namibia and South Africa. *Journal of African Earth Sciences*, **29**, 33–49.

Barbosa, O. and Gomes, F.A. (1958) Pesquisa de Petróleo na Bacia do Rio Corumbataí, Estado de São Paulo. *Divisão de Geologia e Mineralogia do DNPM, Boletim*, **171**, 40 pp.

Beaufort, D. and Meunier A. (1994) Saponite, corrensite and chlorite-saponite mixed-layers in the Sancerre-Couy deep drill-hole (France). *Clay Minerals*, **29**, 47–61.

Bouchet, A., Lajudie, A., Rassineux, F., Meunier, A., and Atabek, R. (1992) Mineralogy and kinetics of alteration of a mixed-layer kaolinite/smectite in nuclear waste disposal

simulation experiment (Stripa site, Sweden). *Applied Clay Science*, **7**, 113–123.

Bristow, T.F., Kennedy, M.J., Derkowski, A., Droser, M.L., Ganjing, J., and Creaser, R.A. (2009) Mineralogical constraints on paleoenvironments of the Ediacaran Doushantuo Formation. *Proceedings of the National Academy of Sciences*, **106**, 13190–13195.

Calarge, L.M., Meunier, A., and Formoso, M.L.L. (2003) A bentonite bed in the Aceguá (RS, Brazil) and Melo (Uruguay) areas: a highly crystallized montmorillonite. *Journal of South American Earth Sciences*, **16**, 187–198.

Calarge, L.M., Meunier, A., Lanson, B., and Formoso, M.L.L. (2006) Chemical signature of two Permian volcanic ash deposits within a bentonite bed from Melo, Uruguay. *Anais da Academia Brasileira de Ciências*, **78**, 525–541.

Catuneanu, O., Wopfner, H., Eriksson, P.G., Cairncross, B., Rubidge, B.S., Smith, R.M.H., and Hancox, P.J. (2005) The Karoo basins of south-central Africa. *Journal of African Earth Sciences*, **43**, 211–253.

Chamley, H. (1989) *Clay Sedimentology*. Springer-Verlag, Berlin, 623 pp.

Colin, F., Nahon, D., Trescases, J.J., and Melfi, A.J. (1990) Lateritic weathering of pyroxenites at Niquelandia, Goias, Brazil: The supergene behavior of nickel. *Economic Geology*, **85**, 1010–1023.

Costa, H.F., Soares A.L., and Magalhães L.F. (1981) *Projeto Rochas Sedimentares – Geologia da Frente Mineiros/ Portelândia*. Goiânia, METAGO, Relatório de Etapa, Brazil, 35 pp.

Coutinho, J.M.V. and Hachiro, J. (2005) Distribution, mineralogy, petrography, provenance and significance of Permian ash-carrying deposits in the Paraná Basin. *Revista do Instituto de Geociências da USP*, **5**, 29–39.

Coutinho, J.M.V., Hachiro, J., Coimbra, A.M., and Santos, P.R. (1988) Ash fall-derived vitroclastic tuffaceous sediments in the Permian of the Paraná Basin and their provenance. Pp. 147–160 in: *Gondwana Seven Proceedings* (H.E. Ulbrich and A.C. Rocha Campos, editors). Instituto de Geociências-USP, São Paulo, Brazil.

Cuevas, J., Villa, R.V., Ramirez, S., Petit, S., Meunier, A., and Leguey, S. (2003) Chemistry of Mg smectites in lacustrine sediments from the Vilcaro Sepiolite Deposit, Madrid Neogene Basin (Spain). *Clays and Clay Minerals*, **51**, 457–472.

Dampare, S.B., Asiedu, D.K., Osae, S., Nyarko, B.J.B., and Banoeng-Yakubo, B. (2005) Determination of rare earth elements by neutron activation analysis in altered ultramafic rocks from the Akwatia district of the Birim diamontiferous field, Ghana. *Journal of Radioanalytical and Nuclear Chemistry*, **265**, 101–106.

Dardenne, M.A. (2000) The Brasília Fold Belt. Pp. 231–263 in: *Tectonic Evolution of South America* (U.G. Cordani, E.J. Milani, A. Thomaz Filho, and D.A. Campos, editors). Fólio Produção Editorial, Rio de Janeiro, Brazil.

Decarreau, A., Petit, S., Vieillard, P., and Dabert, N. (2004) Hydrothermal synthesis of aegirine at 200ºC. *European Journal of Mineralogy*, **16**, 85–90.

Desprairies, A. and Bonnot-Courtois, C. (1980) Relation entre la composition des smectitite d'alteration sous-marine et leur cortege de terres rares. *Earth and Planetary Science Letters*, **48**, 124–130.

De Wit, M., Jeffrey, M., Bergh, H., and Nicolaysen, L. (1988) *Geological map of sectors of Gondwana reconstructed to their disposition ca. 150 Ma*. American Association of Petroleum Geologists, Tulsa, Oklahoma, USA.

Dos Anjos, C.W.D. (2003) A influência térmica de intrusões ígneas sobre pelitos e rochas carbonáticas da Formação Irati, em Goiás. Dissertação de Mestrado, Univ. de Brasília, Brasília, Brazil, 101 pp.

Eggleton, R.A. and Boland, J.N. (1982) Weathering of enstatite to talc through a sequence of transitional phases. *Clays and Clay Minerals*, **30**, 11–20.

Evensen, N.M., Hamilton, P.J., and O'Nions, R.K. (1978) Rare earth abundances in chondritic meteorites. *Geochimica et Cosmochimica Acta*, **42**, 1199–1212.

Farmer, V.C. (1974) The layer silicates. Pp. 331–365 in: *The Infrared Spectra of Minerals* (V.C. Farmer, editor). Monograph **4**, Mineralogical Society, London.

Fontanaud, A. and Meunier, A. (1983) Mineralogical facies of a weathered serpentinized lherzolite from the Pyrenees, France. *Clay Minerals*, **18**, 77–88.

Furquim, S.A.C., Graham, R.C., Barbiero, L., Queiroz Neto, de J.P., and Vallès, V. (2008) Mineralogy and genesis of smectites in an alkaline-saline environment of Pantanal wetland, Brazil. *Clays and Clay Minerals*, **56**, 579–595.

Girardi, V.A.V., Melfi, A.J., and Amaral, S.E. (1978) Efeitos termais associados aos diabasios mesozóicos da Bacia do Paraná. *Boletim do Instituto de Geociências da USP*, **9**, 47–55.

Gomes, J.B.P. (1959) Algumas observações sobre as intrusões de diabásio na Bacia Sedimentar do Paraná. *Boletim Técnico da Petrobrás*, **2**, 7–12.

Goodman, B.A., Russell, J.D., Fraser, A.R., and Woodhams, F.W.D. (1976) A Mössbauer and IR spectroscopic study of the structure of nontronite. *Clays and Clay Minerals*, **24**, 53–59.

Grauby, O., Petit, S., Decarreau, A., and Baronnet, A. (1994) The nontronite-saponite series: An experimental approach. *European Journal of Mineralogy*, **6**, 99–112.

Gromet, L.P., Dymek, R.F., Haskin, L.A., and Korotev, R.L. (1984) The "North American shale composite": Its composition, major and trace element characteristics. *Geochimica et Cosmochimica Acta*, **48**, 2469–2482.

Hein, J.R. and Scholl, D.W. (1978) Diagenesis and distribution of late Cenozoic volcanic sediment in the southern Bering Sea. *Geological Society of America Bulletin*, **89**, 197–210

Hover, V.C., Walter, L.M., Peacor, D.R., and Martini, A.M. (1999) Mg-smectite authigenesis in a marine evaporative environment, salina Ometepec, Baja California. *Clays and Clay Minerals*, **47**, 252–268.

Karakaya, N., Karakaya, M.Ç., Temel, A., Küpeli, Ş., and Tunoğlu, C. (2004) Mineralogical and chemical characterization of sepiolite occurrences at Karapinar (Konya basin, Turkey). *Clays and Clay Minerals*, **52**, 495–509.

Kastner, M. (1999) Oceanic minerals: Their origin, nature of their environment and significance. *Proceedings of the National Academy of Sciences*, **96**, 3380–3387.

Kay, S., Ramos, V.A., Mpodozis, C., and Sruoga, P. (1989) Late Paleozoic to Jurassic silicic magmatism at the Gondwanaland margin: analogy to the Middle Proterozoic in North America? *Geology*, **17**, 324–328.

Keeling, J.L., Raven, M.D., and Gates, W.P. (2000) Geology and characterization of two hydrothermal nontronites from weathered metamorphic rocks at the Uley Graphite Mine, South Australia. *Clays and Clay Minerals*, **48**, 537–548.

Kemp, S.J., Rochelle, C.A., and Merriman, R.J. (2005) Back-reacted saponite in Jurassic mudstones and limestones intruded by a Tertiary sill, Isle of Skye. *Clay Minerals*, **40**, 263–282.

Keyser, N. and Zawada, P.K. (1988) Two occurrences of ash-flow tuff from the lower Beaufort Group in the Heilbron–Frankfort area, northern Orange Free State. *South African Journal of Geology*, **91**, 509–521.

Khoury, H.N., Eberl, D.D., and Jones, B.F. (1982) Origin of magnesium clays from the Amargosa desert, Nevada. *Clays and Clay Minerals*, **30**, 327–336.

Kontak, D.J., Clark, A.H., Farrar, E., Archibald, D.A., and Baadsgaard, H. (1990) Late Paleozoic-early Mesozoic

magmatism in the Cordillera de Carabaya, Puno, southeastern Peru: Geochronology and petrochemistry. *Journal of South American Earth Sciences*, **3**, 213–230.

Lanson, B. (1997) Decomposition of experimental X-ray diffraction patterns (profile fitting): a convenient way to study clay minerals. *Clays and Clay Minerals*, **45**, 132–146.

MacGregor, J.H. (1908) Mesosaurus Brasiliensis nov. sp. do Permiano do Brasil. Pp. 301–336 in: *Relatório da Comissão de Estudos das Minas de Carvão de Pedra do Brasil, por I. C. White*. DNPM, Edição Fac-Similar 1988, Brasília.

Matos, S.L.F., Yamamoto, J.K., Riccomini, C., Hachiro, J., and Tassinari, C.C.G. (2001) Absolute dating of Permian ash-fall in the Rio Bonito Formation, Paraná Basin, Brazil. *Gondwana Research*, **4**, 421–426.

Maynard, J.B., Chocyk, J.M., Gaines, R.R., Krekeler, M.P., Prokopenko, M., Summers, A.M., and Huff, W.D. (1996) Bentonites in the Late Permian (Tatarian) Irati Formation of Brazil: geochemistry and potential of stratigraphic correlation. Pp. 280 in: Geological Society of America Annual Meeting, **28**, Denver, Colorado, Abstracts.

McLachlan, I.R. and Jonker, J.P. (1990) Tuff beds in the northwestern part of the Karoo Basin. *South African Journal of Geology*, **93**, 329–338.

Mendes, J.C., Fúlfaro, V.J., Amaral, S.E., and Landim, P.M.B. (1966) A Formação Irati (Permiano) e fácies associadas. *Boletim da Sociedade Brasileira de Geologia*, **15**, 23–43.

Meunier, A. (2005) *Clays*. Springer, Berlin.

Meunier, A., Lanson, B., and Velde, B. (2004) Composition variation of illite-vermiculite-smectite mixed-layer minerals in a bentonite bed from Charente (France). *Clay Minerals*, **39**, 317–332.

Milani, E.J. (1997) Evolução tectono-estratigráfica da Bacia do Paraná e seu relacionamento com a geodinâmica Fanerozóica do Gondwana sul-ocidental. Tese de Doutorado, Univ. Federal do Rio Grande do Sul, Porto Alegre, Brazil, 255 pp.

Milani, E.J. and Thomaz Filho, A. (2000) Sedimentary Basins of South America. Pp. 389–449 in: *Tectonic Evolution of South America* (U.G. Cordani, E.J. Milani, A. Thomaz Filho, and D.A. Campos, editors). In-Fólio Produção Editorial, Rio de Janeiro, Brazil.

Nahon, D., Colin, P., and Tardy, Y. (1982) Formation and distribution of Mg-Fe-Mn-smectites in the first stages of the lateritic weathering of forsterite and tephroite. *Clay Minerals*, **17**, 339–348.

Noack, Y. and Duplay, J. (1983) Talc and the weathering hydrothermal alteration boundary. *Sciences Géologiques Memoires*, **72**, 121–130.

Noack, Y., Colin, F., Nahon, D., Delvigne, J., and Michaux, L. (1993) Secondary-mineral formation during natural weathering of pyroxene: review and thermodynamic approach. *American Journal of Science*, **293**, 111–134.

Petit, S., Martin, F., Wiewióra, A., De Parseval, P., and Decarreau, A. (2004) Crystal-chemistry of talc: A near infrared (NIR) spectroscopy study. *American Mineralogist*, **89**, 319–326.

Petri, S. and Fúlfaro, V.J. (1983) *Geologia do Brasil*. Editora da Universidade de São Paulo, São Paulo, Brazil.

Pimentel, M.M., Fuck, R.A., Jost, H., Ferreira Filho, C.F., and Araújo, S.M. (2000) The Basement of the Brasília Fold Belt and the Goiás Magmatic Arc. Pp. 195–229 in: *Tectonic Evolution of South America* (U.G. Cordani, E.J. Milani, A. Thomaz Filho, and D.A. Campos, editors). In-Fólio Produção Editorial, Rio de Janeiro, Brazil.

Piper, D.Z. (1974) Rare earth elements in the sedimentary cycle: A summary. *Chemical Geology*, **14**, 285–304.

Ramos, A.N. and Formoso, M.L.L. (1976) Clay mineralogy of the sedimentary rocks of the Paraná Basin, Brazil. *Revista Brasileira de Geociências*, **6**, 15–42.

Ramos, V.A. (2000) The Southern Central Andes. Pp. 561–604 in: *Tectonic Evolution of South America* (U.G. Cordani, E.J. Milani, A. Thomaz Filho, and D.A. Campos, editors). In-Fólio Produção Editorial, Rio de Janeiro, Brazil.

Rehim, H.A.A.A., Mizusaki, A.M.P., Carvalho, M.D., and Monteiro, M. (1986) Talco e Estevensita na Formação Lagoa Feia da Bacia de Campos – Possíveis implicações no ambiente deposicional. *Anais do Congresso Brasileiro de Geologia*, **34**, 416–425.

Reynolds, R.C. (1980) Interstratified Clay Minerals. Pp. 249–303 in: *Crystal Structures of Clay Minerals and their X-ray Identification* (G.W. Brindley and G. Brown, editors). Monograph **5**, Mineralogical Society, London.

Reynolds, R.C. (1985) *NEWMOD, A Computer Program for the Calculation of One-Dimensional Diffraction of Mixed-layer Clays*. Published by the author, Hanover, New Hampshire, USA.

Rodrigues, A.R. (2001) *Projeto Calcário Montividiu*. Relatório Final de Pesquisa, METAGO, Goiânia, Brazil, 16 pp.

Rodrigues, R. and Quadros, L.P. (1976) Mineralogia de argilas e teor de Boro das formações paleozóicas da Bacia do Paraná. *Anais do Congresso Brasileiro de Geologia*, **29**, 351–379.

Sakharov, B.A., Dubińska, E., Bylina, P., Kozubowski, J.A., Kaprón, G., and Frontczak-Baniewicz, M. (2004) Serpentine-smectite interestratified minerals from Lower Silesia (SW Poland). *Clays and Clay Minerals*, **52**, 55–65.

Sanford, R.M. and Lange, F.W. (1960) Basin-study approach to oil evaluation of Paraná Miogeosyncline, south Brazil. *American Association of Petroleum Geologists Bulletin*, **44**, 1316–1370.

Santos, R.V., Dantas, E., Alvarenga, C.J.S., Berdran, F., Reis, W., Guimarães, E.M., Oliveira, C.G., Marques-Toigo, M., Mendonça Filho, J.G., Dos Anjos, C.W.D., and Medeiros, S.R. (2003) Geochemical and thermal effects of basic intrusive rocks on sediments from the Irati Formation – northwestern Paraná Basin. *Short Papers of the South American Symposium on Isotope Geology*, **4**, 776–779.

Santos, R.V., Sousa, P.A., Alvarenga, C.J.S., Dantas, E.L., Pimentel, M.M., Oliveira, C.G., and Araújo, L.M. (2006) SHRIMP U-Pb Zircon dating and palinology of bentonitic layers from the Permian Irati Formation: Stratigraphic implications for southwestern Gondwana. *Gondwana Research*, **9**, 456–463.

Santos Neto, E.V. (1993) Caracterização Geoquímica e Paleoambiente Deposicional da Sequência Carbonato-Pelítica Superior do Membro Assistência, Formação Irati no Estado de São Paulo, Bacia do Paraná. Dissertação de Mestrado, Univ. Federal do Rio de Janeiro, Rio de Janeiro, Brazil, 203 pp.

Sempere, T., Carlier, G., Soler, P., Fornari, M., Carlotto, V., Jacay, J., Arispe, O., Néraudeau, D., Cárdenas, J., Rosas, S., and Jiménez, N. (2002) Late Permian–Middle Jurassic lithospheric thinning in Peru and Bolivia, and its bearing on Andean-age tectonics. *Tectonophysics*, **345**, 153–181.

Stollhofen, H., Stanistreet, I.G., Bangert, B., and Grill, H. (2000) Tuffs, tectonism and glacially related sea-level changes, Carboniferous–Permian, southern Namibia. *Palaeogeography, Palaeoclimatology, Palaeoecology*, **161**, 127–150.

Tardy, Y. (1997) *Petrology of Laterites and Tropical Soils*. Balkema, Amsterdam.

Taylor, S.R. and McLennan, S.M. (1985) *The Continental Crust: Its Composition and Evolution*. Blackwell, Oxford, UK.

Traoré, D, Beauvais, A., Chabaux, F., Peiffert, C., Parisot, J.C., Ambrosi, J.P., and Colin, F. (2008) Chemical and physical transfers in an ultramafic rock weathering profile: Part 1. Supergene dissolution of Pt-bearing chromite. *American*

Mineralogist, **93**, 22–30.
Velde, B., and Meunier, A. (2008) *The Origin of Clay Minerals in Soils and Weathered Rocks*. Springer-Verlag, Berlin.
Viljoen, J.H.A. (1995) Piroklastiese afsettings von permouder-dom in die hoof-karookom. PhD thesis, Stellenbosch University, South Africa, 248 pp.
White, D. (1908) Flora Fóssil das Coal Measures do Brasil. Pp. 337–617 in: *Relatório da Comissão de Estudos das Minas de Carvão de Pedra do Brasil, por I. C. White*. DNPM, Edição Fac-Similar 1988, Brasília.
Whitney, G. (1983) Hydrothermal reactivity of saponite. *Clays and Clay Minerals*, **31**, 1–8.
Wilkins, R.W.T. and Ito, J. (1967) Infrared spectra of some synthetic talcs. *American Mineralogist*, **52**, 1649–1661.
Winchester, J.A. and Floyd, P.A. (1977) Geochemical discrimination of different magma series and their differentiation products using immobile elements. *Chemical Geology*, **20**, 325–343.
Yalçin, H. and Bozkaya, O. (2006) Mineralogy and geochemistry of Paleocene ultramafic- and sedimentary-hosted talc deposits in the southern part of the Sivas Basin, Turkey. *Clays and Clay Minerals*, **54**, 333–350.

(*Received 9 November 2009; revised 8 September 2010; Ms. 381; A.E. R.J. Pruett*)